Thermal Screening Masses in the Standard Model of Strong and Electroweak Interactions

Dissertation
zur Erlangung des Doktorgrades
der Fakultät für Physik
der Universität Bielefeld

vorgelegt von
Jörn Rank

16. Januar 1998

Contents

List of Figures

List of Tables

Chapter 1

Introduction

Todays understanding of physics classifies the fundamental forces that determine the behaviour of matter and its constituents into four classes, the gravitation, the electromagnetism, the weak and the strong force. From these, the weak and the strong force are of central meaning for the interaction between quarks and gluons.

The theoretical description of the interaction between elementary particles is known in principle for about 30 years. Based on the outstanding works from Glashow [1], Weinberg [2] and Salam [3] the standard model (SM) of strong and electroweak interactions was formulated. Because of the complex structure of the SM it was until now only possible to study a few aspects of the SM, most of them within the framework of perturbation theory. In the energy ranges investigated so far the experimental observations agree very precisely with the predictions of the SM. As a consequence, the SM has established as the description of the strong and electroweak interactions.

The SM includes several non-perturbative ideas, for instance confinement, spontaneous symmetry breaking or the Higgs mechanism (for an overview, see e.g. [4]). They lead to phenomena that can not be described by perturbative methods. Remedy is provided by the lattice discretized version of the theory which was proposed by Wilson in his famous work [5]. Based on this, computer simulations of aspects the SM became a very powerful tool to investigate the SM beyond perturbation theory [6].

It is expected that, at very high temperature (and/or pressure), phase transitions occur which lead into a regime in which the behaviour between elementary particles changes qualitatively. The non-perturbative aspects of the SM at low temperature like confinement vanish at the critical temperature. On the other hand, additional,

non-perturbative features like the creation of thermal masses, their screening be-
haviour and the interaction based on excitations of quasi-particles occur in the high
temperature phase. This phase is widely unexplored until now. Therefore a de-
tailed theoretical understanding of the temperature dependent features of the SM
is essential to estimate conditions for new experiments.

Experimentally, high temperatures (and/or pressures) correspond to high energies.
As a consequence, thermodynamic studies offer the possibility to investigate the
range of validity of the SM.

So far, the deconfinement phase transition was investigated very intensively. It
separates the low temperature phase, in which the quarks and gluons can only exist
in bounded, colourless states, from the high temperature phase, in which quarks and
gluons decouple and form a quark gluon plasma.

An investigation of the electroweak phase transition with parameter values close to
the physical weak coupling regime, however, started only recently at the beginning
of the nineties (see e.g. [7]). The $SU(2)$ Lagrangian of the SM is broken for low tem-
peratures, so that the quarks, leptons, $W^{\pm}$–bosons and the Z–boson become massive
particles. For temperatures above the critical temperature of the electroweak phase
transition the $SU(2)$–symmetry is restored. In the theory this becomes obvious by
the vanishing vacuum expectation value of the Higgs field. If and how several ob-
servables might change at the electroweak phase transition is widely unexplored so
far. It is expected, for example, that the baryon surplus in the universe can be
explained by non-equilibrium processes at the electroweak phase transition if the
latter is strong enough of first order.

A fundamental concept within the description of the behaviour of particles in a ther-
mal medium is the temperature dependent mass or screening mass. It is generated
by the interaction of a particle with the medium. A detailed understanding of the
screening masses of the fundamental constituents of the SM (quarks, gluons, leptons,
$W^{\pm}$–bosons, Z–boson, Higgs-boson) is of essential meaning both for a discussion of
the physics of the high temperature phase of the SM and for a discussion of possible
experimental observable consequences.

One possibility to determine screening masses and to compare the results with
perturbative calculations is the direct computation of the propagators of the con-
stituents. As these objects are gauge dependent one has to work in a fixed gauge.
In this work we have chosen the Landau gauge.

As noted above, screening masses occur in several energy ranges of the SM. In the
energy region dominated by the strong interaction thermal masses occur both in
the electric (temporal) and in the magnetic (spatial) sector of the theory. It was

shown [8] that the gluonic screening masses influence strongly the infrared sector of the theory. The electric screening mass is known in lowest order perturbation theory for a long time, $m_e = \sqrt{N_c/3 + N_f/6} \; g(T)\,T$. This temperature dependence is sufficient to cure infrared divergences of $\mathcal{O}(gT)$. The situation for the magnetic mass is more difficult. As all orders of perturbation theory would contribute equally, a perturbative expression for the magnetic mass does not exist. However, a dependence of the form $m_m \sim g^2 T$ is widely believed as this would cure higher order infrared divergences of $\mathcal{O}(g^2 T)$. Moreover, if the magnetic mass indeed does not vanish it contributes in next-to-leading order to m_e [9, 10]. Therefore also m_e has to be treated non-perturbatively beyond leading order.

In the electroweak sector of the theory the screening behaviour of the W-boson is of special interest. Like in the case of gluonic screening masses, the leading order behaviour in the electric sector is $\mathcal{O}(gT)$. Equally, the magnetic W-boson screening mass is entirely of non-perturbative origin and expected to be $\mathcal{O}(g^2 T)$. However, a non-vanishing magnetic mass is not only interesting for a better understanding of the infrared behaviour of the theory. It is furthermore expected that the magnitude of a thermal magnetic W-boson mass determines the strength of the electroweak phase transition [11, 12].

To summarize the above, thermal screening masses play an important role in the high temperature phase of the standard model of strong and electroweak interactions. An investigation of these masses requires non-perturbative methods. In this work we present results obtained from Monte Carlo simulations of the lattice regularized version of the standard model.

For a qualitative overview of the temperature dependence of the screening masses it is sufficient to investigate not the full standard model but simplified models of the two energy ranges of interest. The full theory of the strong interaction is Quantum-chromodynamics (QCD). It is a gauge theory based on the group $\mathrm{SU}(N_c)$ with $\mathrm{N}_c{=}3$ being the number of colours. As computer simulations of full QCD are very time consuming, we have investigated pure $\mathrm{SU}(2)$ lattice gauge theory. This model neglects dynamical fermions, $N_f = 0$, and the number of colours is reduced to two. $\mathrm{SU}(2)$ is the smallest, non-abelian, unitary group and yields qualitatively the same properties as $\mathrm{SU}(3)$, i.e. asymptotic freedom, confinement etc. A simplified description of the electroweak sector of the standard model is given by the $\mathrm{SU}(2)$-gauge-Higgs model. Again, dynamical fermions are not taken into account. Furthermore, the abelian subgroup of the full $\mathrm{SU}(2){\otimes}\mathrm{U}(1)$ symmetry is neglected.

This dissertation summarizes the work that was done in collaboration with U.M. Heller and F. Karsch [13]-[15] and with F. Karsch, T. Neuhaus and A. Patkós [16]-[18], respectively. In the next chapter we discuss the basic concepts and conceptual difficulties of thermal screening masses. We summarize results for the gluon screening

masses, known from perturbation theory, and results for the W-boson screening mass, based on gap equations. Furthermore we present the correlation functions that we have used to determine the screening masses. In Chap. 3 we deal with pure SU(2) lattice gauge theory. After a general discussion we summarize some technical aspects, i.e. the Wilson action and a tree-level Symanzik improved action and the procedure followed to fix the relation between bare gauge couplings and the temperature. Finally we shortly discuss the deconfinement phase transition. Chap. 4 is concerned with the SU(2)-gauge-Higgs model. In this context we point out the basic concepts of dimensional reduction and present an action for the effective 3-dimensional theory. We discuss the electroweak phase transition and present the method of measuring Lee-Yang zeros to estimate the critical Higgs mass at which the phase transition looses its first order character. Our numerical results are presented and discussed in Chap. 5. At last, we give our conclusions in Chap. 6.

The appendix covers two topics. Part A is about the determination of screening masses on the lattice. As it is of more technical nature, we have separated it from the remaining thesis. In App. B we discuss lattice gauge fixing methods. At first we recall how to fix the Landau gauge on the lattice. Finally, a method of fixing a more general gauge – the covariant gauge – on the lattice is presented.

Chapter 2

Screening Masses - Theoretical Background

The main purpose of this dissertation is an investigation of thermal gauge boson screening masses. In the context of pure SU(2) gauge theory and the SU(2)-gauge-Higgs model we want to obtain a better understanding of the temperature behaviour of these masses. Especially for the electric screening mass we want to check if we get in contact with perturbative predictions in the temperature regime under consideration. For a systematic discussion of these points we present in this chapter the theoretical background of screening masses only. Our numerical results are summarized separately in Chap. 5.

The next section deals with the basic concepts of screening masses. We point out the difficulties that arise already in finding a meaningful definition of a screening mass and summarize the work that was done to solve this problem. In Sec. 2.2 we present gauge dependent and alternatively gauge independent correlation functions that can be used to extract screening masses from a lattice calculation. Some analytical calculations for the screening masses are presented in Sec. 2.3. We discuss the gluon screening masses within perturbation theory and give, for the electric screening mass, the lowest order and next-to-leading order perturbative results. Furthermore we quote results for the magnetic screening mass in the SU(2)-gauge-Higgs model, based on gap equations.

2.1 Basic Concepts and Conceptual Difficulties

The high temperature deconfined phase of QCD, in which the quarks and the gluons decouple and form a quark gluon plasma, is characterized by the occurrence of

chromo-electric and -magnetic screening masses which control the infrared behaviour of the theory. The electric screening mass, m_e, is responsible for the Debye screening of the heavy quark potential. Its temperature dependence is known for a long time in lowest order perturbation theory, $m_e \sim gT$ [19]. It was shown in [8] that this is sufficient to cure infrared divergences of the theory of momentum scales of $\mathcal{O}(gT)$. However, it is pointed out in various articles (see for instance [20]-[22] and [23, 24]) that in the usual temperature range of investigation, i.e. slightly above the critical temperature of the deconfinement phase transition, m_e deviates strongly from its lowest order perturbative prediction. On the other hand, the magnitude of m_e influences strongly the existence or non-existence of hadronic bound states in the high temperature phase. It is therefore essential for any further analysis of the quasi-particle excitation spectrum in the QCD plasma phase to understand the temperature dependence of the electric screening mass quantitatively.

The discussion of the magnetic mass, m_m, is much more difficult. It was shown in [25] that it vanishes at lowest order perturbation theory. Furthermore one can show that a non-vanishing magnetic mass has to be entirely of non-perturbative origin as every order in perturbation theory would contribute equally [8]. As a consequence, only little is known about the temperature dependence of m_m so far, even on a qualitative level. Following the discussion in [8], a magnetic mass of the form $m_m \sim g^2T$ is sufficient to cure the remaining infrared divergences of the theory of $\mathcal{O}(g^2T)$. Very recently, however, a mechanism was suggested which is able to cure these divergences also without the dynamic generation of a magnetic mass [26]. Despite this possibility it is widely believed that the magnetic mass obeys a non-vanishing value at high temperature. This assumption is strengthened by investigations through the analysis of gap equations [11, 12], [27]-[29] and several non-perturbative approaches [30, 31], even if the latter yield other functional dependencies than the expected g^2T-behaviour. Finally, the assumption of a non-vanishing magnetic mass also influences the perturbative calculation of the electric mass. If one indeed should find $m_m \sim g^2T$, than the next-to-leading order correction to m_e is of $\mathcal{O}(g^2 \ln g)$ [9, 10].

We have seen that screening masses are essentially of non-perturbative origin. However, one can use them to remove some problems that arise in the perturbative treatment of the thermodynamics of the plasma phase [32]. For instance, the equation of state for SU(3) gauge theory is quite well known from lattice calculations. One finds that the energy density and the pressure are, even at rather high temperatures ($T \simeq 5\,T_c$), about 10 - 15 % below the ideal gas limit [33]. One might expect that these deviations become smaller by taking higher order perturbative corrections into account. However, the situation is getting worse, as the coefficients of the weak coupling expansion of the free energy density are of alternating sign and increasing magnitude (see [32] and references therein). Remedy might be provided by so-called screened perturbation theory [32]. The idea is not to expand around the massless ideal gas limit but to perform the loop expansion starting from a massive ideal gas.

For the simple case of the N component scalar Φ^4-theory the power of this method was demonstrated in [32]. In Fig. 2.1 one can see the free energy density F, normal-
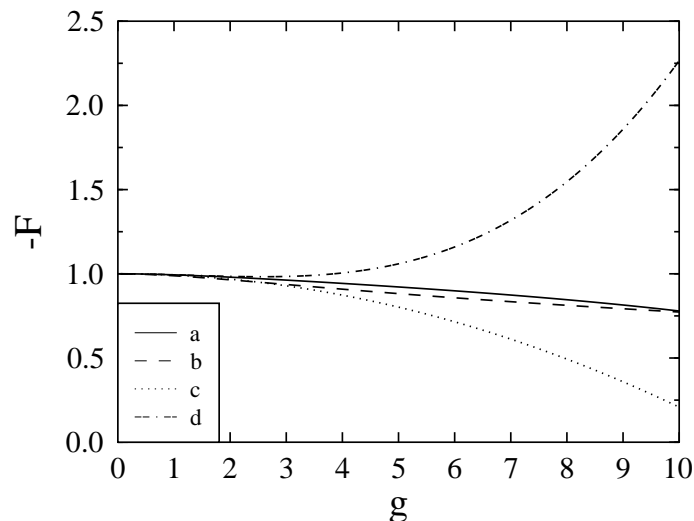
Figure 2.1: Normalized free energy density of the scalar Φ^4-theory as a function of the scalar self-coupling g [32]. See text for details.

ized to the Stefan Boltzmann value of a massless ideal gas, $F_{SB} = \pi^2 T^4/90$. The curves (a) and (b) represent 2-loop and 1-loop results of the screened loop expansion. Also at large values of the coupling they are lying very close to the theoretical value. Furthermore, the situation gets improved if one goes from a 1-loop to 2-loop calculation. In contrast, the failure of a conventional perturbative expansion can be seen from the curves (c) and (d), which show the $\mathcal{O}(g^2)$ and $\mathcal{O}(g^3)$ results.

Not only the temperature dependence of the screening masses is complicated, also their exact definition is not without problems. In general, screening masses are related to the low momentum behaviour of the static sector ($p_4 = 0$) of the gauge boson polarization tensor, $\Pi_{\mu\mu}(\vec{p}, p_4)$. As $\Pi_{\mu\mu}$ is gauge dependent, it is not obvious that any quantity extracted from it would have a physical, i.e. gauge invariant meaning. For example, the former zero momentum limit definition of the screening masses, $m_{\mu,\text{old}}^2 = \Pi_{\mu\mu}(|\vec{p}| \to 0, p_4 = 0)$, yields masses which depend on the gauge in which $\Pi_{\mu\mu}$ is calculated. This problem was cured by the definition introduced in [34, 35], $m_\mu^2 = \Pi_{\mu\mu}(\vec{p}^{\,2} = -m_\mu^2, 0)$. These so-called pole masses are, within a wide class of gauges, gauge invariant to arbitrary order in perturbation theory. Even if one has to calculate the corresponding correlation functions in a fixed gauge, the pole masses extracted from them will be gauge independent. At this point we want to introduce the agreement that, whenever we are talking in the following about measuring a gauge dependent quantity in a fixed gauge, we imply that we are using

the Landau gauge, $|\partial_\mu A^\mu(x)|^2 = 0$. This gauge has the advantage that it is covariant and easy to realize on the lattice. A detailed discussion on it is given in App. B.

Let us return to the discussion of the pole mass definition of the screening masses. Another great advantage of it is given by the fact that the exponential decay of finite temperature gauge boson correlation functions at large spatial separations yields exactly these pole masses. Therefore they are well suited candidates for an investigation based on lattice Monte Carlo methods.

An alternative way to define screening masses is through the use of gauge invariant operators. If one is interested in the electric screening mass only, typical candidates are Polyakov loop correlation functions which are related to the heavy quark potential at finite temperature. But one may think also about other observables as long as they project onto states with the correct quantum numbers. Some were introduced in [36] and used in the so-called SU(2) + adjoint Higgs theory [23, 24]. This model is based on dimensional reduction and describes the high temperature phase of QCD. However, it is not clear in how far screening masses, defined through gauge invariant operators, agree with the corresponding pole masses from the gauge boson propagator. For example, an investigation of gauge invariant glueball operators with the quantum numbers of the gluon within pure SU(2) gauge theory [37] yields screening masses which are much larger than the corresponding masses obtained directly from the gluon propagator in Landau gauge [22], [13]-[15]. However, this result is not surprising as the gauge invariant correlation functions, which correspond to glueball states at low temperature, describe "melted" glueball states, i.e. states of several decoupled gluons, at high temperature. These states have an effective thermal mass which is, of course, much larger than the thermal screening mass of a single gluon. Similar observations have been made in a very recent study [29] of the electroweak sector of the theory, in which the screening masses of the Higgs boson and of the W-boson were investigated. It also opens the possibility that masses, extracted from gauge invariant operators, project onto superpositions of several elementary gauge boson excitations, i.e. onto quasi-particle states. This leads again to the discussion of the physical meaning of the screening masses. The central point is whether the QCD plasma phase has to be described by colourless excitations only, or if quarks and gluons are the basic degrees of freedom. For example, the latter is preferred by calculations of the QCD equation of state.

Let us now discuss the screening behaviour in the electroweak sector in which very similar phenomena and questions arise. One again defines screening masses in the electric and magnetic sectors. Like in QCD, the leading order electric screening mass is of $\mathcal{O}(gT)$. Much more interesting than the electric screening mass is now its magnetic counterpart. A non-vanishing magnetic screening mass – if existing – does not only control the infrared behaviour of the electroweak theory, its magnitude furthermore influences the existence or non-existence of the first order character of

the electroweak phase transition [11, 12]. Again, the temperature dependence of the magnetic W-boson screening is not known, but similar considerations as made in QCD give rise to an expected behaviour of $m_W \sim g^2 T$.

Due to the lack of a perturbative treatment of the W-boson screening mass, alternative approaches are needed. In [38]-[41] several Monte Carlo calculations concerning W-boson screening masses as well as Higgs masses are presented. Whereas these results are obtained from gauge invariant correlation functions, the authors in [28, 29, 42] use, similar to the treatment of the magnetic mass in QCD, a coupled set of gap equations for the scalar and vector propagators on the mass shell. Based on their analysis one might assume that also in the high temperature phase the magnetic W-boson screening mass is generated essentially by a Higgs-type phenomenon. The difference is that the vacuum expectation value of the Higgs field, which plays the role of the order parameter of the theory, is much smaller at high temperature. This can be seen as the motivation for using the same gauge invariant operators for the calculation of the magnetic W-boson mass and of the Higgs mass in the high temperature phase as in the low temperature phase.

To summarize the above discussion, a detailed knowledge of the temperature dependence of the various screening masses arising in QCD and the electroweak theory would help to get insight into the non-perturbative nature of the high temperature phases of quantum field theories and the regularization of infrared divergences appearing in perturbative treatments. One of the central problems still is to give a gauge invariant meaning to the screening masses. Therefore measurements of gauge dependent correlation functions in a fixed gauge should be compared with results from gauge invariant operators. This may provide an answer to the question about the nature of fundamental excitations of the theory in the high temperature phase.

2.2 Measuring Screening Masses on the Lattice

2.2.1 Screening Masses from the Gauge Boson Propagator

As the method of extracting the gluon screening masses from the gluon propagator in SU(2) gauge theory is nearly identical to the one of measuring the W-boson screening masses from the W-boson propagator in the SU(2)-gauge-Higgs model we will discuss in this section the case in general. In the SU(2)-gauge-Higgs model we analyse only the dimensional reduced effective 3-dimensional theory. Therefore all comments on the time direction refer in the following, of course, only to the SU(2) gauge theory. For the SU(2)-gauge-Higgs model one can simply neglect the terms with x_4 or p_4 in all formulas. As a consequence, we can investigate for this model the

screening behaviour in the spatial directions only, i.e. we can not calculate electric W-boson screening masses.

Let us start with the gauge fields $A_\mu(\vec{x}, x_4)$. From this, we define momentum dependent gauge fields,

$$\tilde{A}_\mu(p_\perp, x_3) = \sum_{x_\perp, x_4} e^{i x_\perp p_\perp} A_\mu(x_\perp, x_3, x_4) \quad \mu = 1, \dots, 4 \quad , \tag{2.1}$$

and the corresponding correlation functions,

$$\tilde{G}_\mu(p_\perp, x_3) = \left\langle \mathrm{Tr}\ \tilde{A}_\mu(p_\perp, x_3) \tilde{A}_\mu^\dagger(p_\perp, 0) \right\rangle \quad \mu = 1, \dots, 4 \quad , \tag{2.2}$$

with $x_\perp = (x_1, x_2)$ and $p_\perp = (p_1, p_2)$. On a finite lattice, the momenta are given by $p_i = 2\pi k_i/(a N_i)$, with $k_i = -\frac{1}{2} N_i + 1, \dots, \frac{1}{2} N_i$ and N_i being the length of the lattice in the i-th direction.

The long-distance behaviour of $\tilde{G}$ yields the energies in the electric and magnetic sectors, i.e.

$$\begin{aligned} G_e(p_\perp, x_3) &\equiv& \tilde{G}_4(p_\perp, x_3) \\ &\sim& \exp\{-E_e(p_\perp)\, x_3\} \quad \text{for } x_3 \gg 1 \, , \end{aligned} \tag{2.3}$$

$$\begin{aligned} G_m(p_\perp, x_3) &\equiv& \frac{1}{2}\left(\tilde{G}_1(p_\perp, x_3) + \tilde{G}_2(p_\perp, x_3)\right) \\ &\sim& \exp\{-E_m(p_\perp)\, x_3\} \quad \text{for } x_3 \gg 1 \, . \end{aligned} \tag{2.4}$$

In (2.4) we explicitly use the fact that we want to measure the propagator in Landau gauge. Then $\tilde{G}_3(p_\perp, x_3)$ is independent of x_3 and therefore does not have to be taken into account. For $p_\perp \equiv (0, 0)$ the long-distance behaviour of these correlation functions thus defines electric and magnetic screening masses, which are related to the static sector of the gauge boson polarization tensor,

$$m_\mu^2 = \Pi_{\mu\mu}(\vec{p}^2 = -m_\mu^2, p_4 = 0) \quad . \tag{2.5}$$

We want to emphasize again that these pole masses are, within a wide class of gauges, gauge invariant to arbitrary order in perturbation theory.

We are left to discuss the relation of these formulas to physics on a lattice. As we are dealing with high temperature physics, the lattice distance a becomes very small and the gauge fields are smooth. Therefore we can use the general relation between the gauge fields and the link matrices,

$$U_\mu(x) = \exp\{i g a A_\mu(x)\} \quad , \tag{2.6}$$

to approximate $A_\mu(x)$ on the lattice,

$$A_\mu(x) \simeq \frac{1}{2iga}[(U_\mu(x) - U_\mu^\dagger(x)) - \underbrace{\mathrm{Tr}\,(U_\mu(x) - U_\mu^\dagger(x))}_{= 0 \text{ for } U_\mu(x)\,\in\,\mathrm{SU}(2)}] \quad . \tag{2.7}$$

Using this formula in (2.1) one can then measure the screening masses on the lattice in the way discussed above, Eqs. (2.2) - (2.4).

2.2.2 The Electric Screening Mass from the Singlet Potential

In this subsection we present an alternative way how to extract the electric screening mass (or Debye mass) m_e within QCD with N_c colour degrees of freedom.

For temperatures above the critical temperature T_c the confinement potential between a quark and an anti-quark is replaced by the colour averaged potential [43], which, in lowest order perturbation theory, is of the form

$$V_{\mathrm{av}}(R,T) \sim \frac{1}{T\,R^2}\,e^{\perp 2\,m_e(T)R} \quad \text{for } T > T_c \quad . \tag{2.8}$$

As V_{av} decreases very fast, the numerical signal gets lost in statistical noise in the long distance regime. On the other hand, (2.8) is only valid at large distances. This situation is improved for the colour singlet potential, which is controlled to leading order perturbation theory by 1-gluon exchange and therefore takes on the form

$$V_1(R,T) = -g^2\,\frac{N_c^2 - 1}{8\pi\,N_c} \cdot \frac{e^{\perp m_e(T)R}}{R} \quad \text{for } T > T_c \quad . \tag{2.9}$$

The colour singlet potential, however, is gauge dependent and one again has to fix a gauge before it can be evaluated.

On the lattice one can extract both potentials by measuring Polyakov loop[1] correlation functions [43],

$$e^{\perp V_{\mathrm{av}}(R,T)/T} \;=\; \frac{\langle \mathrm{Tr}\; L(\vec{R})\,\mathrm{Tr}\; L^\dagger(\vec{0}) \rangle}{\langle |L| \rangle^2} \quad , \tag{2.10}$$

$$e^{\perp V_1(R,T)/T} \;=\; N_c\,\frac{\langle \mathrm{Tr}\;(L(\vec{R})\,L^\dagger(\vec{0})) \rangle}{\langle |L| \rangle^2} \quad . \tag{2.11}$$

(2.9) and (2.11) are point-to-point correlation functions. In numerical simulations it is, however, more efficient to use plane-plane correlation functions to extract the electric screening mass. This is done by replacing in (2.11) the expression for the Polyakov loop $L(\vec{R})$ by $L(x_3) \equiv \sum_{x_1,x_2} L(x_1, x_2, x_3)$. Then (2.9) and (2.11) transform into

$$V_{1,\mathrm{sum}}(x_3, T) \sim e^{\perp m_e(T)x_3} \quad \text{for } T > T_c \tag{2.12}$$

and

$$e^{\perp V_{1,\mathrm{sum}}(x_3,T)/T} = N_c\,\frac{\langle \mathrm{Tr}\;(L(x_3)\,L^\dagger(0)) \rangle}{\langle |L| \rangle^2} \quad . \tag{2.13}$$

---

[1] For a definition of the Polyakov loop see Sec. 3.3.

2.2.3   Vector Screening Masses from Gauge Invariant Correlators

In Sec. 2.2.1 we have explained how to obtain the W-boson screening mass from the W-boson propagator. It is, of course, interesting to compare the masses calculated in this way with masses extracted from gauge invariant vector correlation functions. For this purpose we define, similar to Eq. (2.1), the zero momentum field[2]

$$\tilde{O}_{v,i}(x_3) = \sum_{x_\perp} \sigma_3 \, \Phi^\dagger(x_\perp, x_3) \, U_i(x_\perp, x_3) \, \Phi\big((x_\perp, x_3) + \hat{i}\,\big) \quad i = 1, 2 \quad . \tag{2.14}$$

$\Phi(x)$ is a complex 2×2 matrix field. In terms of the real weak isosinglet-triplet decomposition of the complex Higgs doublet it is given by

$$\Phi(\vec{x}) = \Phi_0(\vec{x}) \, \mathbb{1} + i \, \Phi_j(\vec{x}) \, \sigma_j \quad . \tag{2.15}$$

σ_1, σ_2, σ_3 are the Pauli matrices. From (2.14) we have the correlation function

$$\tilde{G}_{v,i}(x_3) = \Big\langle \mathrm{Tr} \, \tilde{O}_{v,i}(x_3) \, \mathrm{Tr} \, \tilde{O}_{v,i}(0) \Big\rangle \quad i = 1, 2 \quad , \tag{2.16}$$

and finally (compare with (2.4))

$$G_v(x_3) \equiv \frac{1}{2} \Big(\tilde{G}_{v,1}(x_3) + \tilde{G}_{v,2}(x_3) \Big) \quad . \tag{2.17}$$

The operator $G_v(x_3)$ projects onto states with zero momentum. Its long distance behaviour yields the mass of a vector particle with the quantum numbers of the W-boson [44]. This mass is a suitable candidate for comparing it with the propagator mass.

2.2.4   The Higgs Boson Screening Mass from the Φ-Propagator

Measuring the Higgs boson screening mass from the Φ-propagator is quite similar to the measurement of gauge boson screening masses from the gauge boson propagator, see Sec. 2.2.1. As we are only interested in zero momentum results and three dimensions, the equivalent expression to Eq. (2.1) is

$$\tilde{\Phi}_i(x_3) = \sum_{x_\perp} \Phi_i(x_\perp, x_3) \quad i = 1, 2 \quad . \tag{2.18}$$

---

[2]In the SU(2)-gauge-Higgs model we are only interested in the three dimensional theory. Therefore we have omitted in the following formulas the time direction.

Next we define the gauge dependent correlation function

$$\tilde{G}_{\Phi,i}(x_3) = \left\langle \mathrm{Tr}\ \tilde{\Phi}_i(x_3)\tilde{\Phi}_i^\dagger(0) \right\rangle \quad i = 1, 2 \quad . \tag{2.19}$$

and finally

$$G_\Phi(x_3) \equiv \frac{1}{2}\left(\tilde{G}_{\Phi,1}(x_3) + \tilde{G}_{\Phi,2}(x_3) \right) \quad . \tag{2.20}$$

The exponential decay of $G_\Phi(x_3)$ at long distances yields the Higgs boson screening mass m_Φ.

2.2.5 Scalar Screening Masses from Gauge Invariant Correlators

In the previous section we have explained how to extract the Higgs boson screening mass from the Φ-Propagator. Similar to the discussion of the W-boson screening mass we want to compare this mass with masses obtained from gauge invariant scalar correlation functions. We start with

$$\tilde{O}_s^\alpha(x_3) = \sum_{i=1}^{2}\sum_{x_\perp} \Phi^\dagger(x_\perp, x_3)\, U_i(x_\perp, x_3)\, \Phi\big((x_\perp, x_3) + \hat{i}\big) \quad . \tag{2.21}$$

Then we define

$$\tilde{G}_s^\alpha(x_3) \;=\; \left\langle \mathrm{Tr}\ \tilde{O}_s^\alpha(x_3)\, \mathrm{Tr}\ \tilde{O}_s^\alpha(0) \right\rangle \quad \text{and} \tag{2.22}$$

$$\tilde{G}_s^\beta(x_3) \;=\; \left\langle \det \Phi(x_3)\ \det \Phi(0) \right\rangle \quad . \tag{2.23}$$

The long distance behaviour of both correlation functions (2.22) and (2.23) gives screening masses in the scalar Higgs channel [45]. We will compare them with the screening mass from the Φ-propagator.

2.3 Analytical Results for Screening Masses

2.3.1 Gluon Screening Masses in Pure SU(N$_c$) Gauge Theory

For SU(N$_c$) gauge theory without dynamical fermions, the lowest order perturbation theory result for the electric screening mass is [25]

$$m_{e,0}(T) = \sqrt{\frac{N_c}{3}}\, g(T)\, T \quad . \tag{2.24}$$

It was shown in lattice perturbation theory [46] that this result is strongly effected by finite cut-off effects, similar to what has been found in [47] for the Stefan Boltzmann law for an ideal gas. For the Wilson action the leading corrections to (2.24) are $\mathcal{O}((aT)^2)$, i.e. $\mathcal{O}(N_\tau^{\perp 2})$. For $N_c = 2$ this is shown in Fig. 2.2. For large N_τ
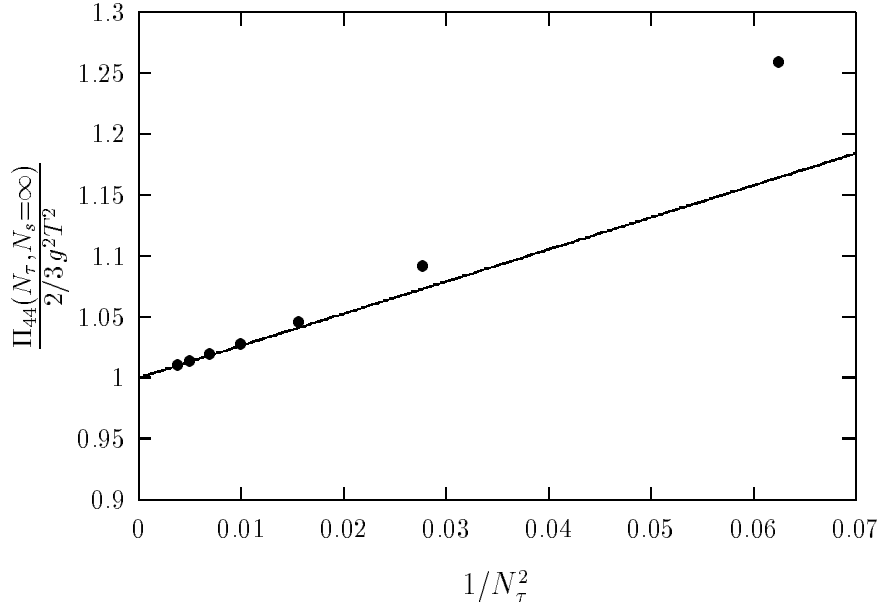
Figure 2.2: The gluon polarization tensor Π_{44} at infinite N_s and various N_τ. The solid line shows the asymptotic result (2.25).

these deviations are due to the $\mathcal{O}(a^2)$ discretization errors introduced in the Wilson formulation. On a spatially infinite lattice we find for these cut-off errors

$$
\begin{aligned}
\frac{\Pi_{44}(N_\tau \to \infty, N_s = \infty)}{2/3\, g^2 T^2} &= 1 + N_\tau^{\perp 2} \frac{1}{40\pi^2} \int_0^\infty dx\, x^5 \frac{\sinh x}{\sinh^4 \frac{x}{2}} + \mathcal{O}(N_\tau^{\perp 4}) \\
&= 1 + \frac{4}{15} \left(\frac{\pi}{N_\tau}\right)^2 + \mathcal{O}(N_\tau^{\perp 4}) \quad .
\end{aligned}
\tag{2.25}
$$

This is similar in magnitude to the cut-off dependence of bulk thermodynamic observables like the energy density [48]. Using an improved action these leading cut-off errors are eliminated and corrections only start at $\mathcal{O}(N_\tau^{\perp 4})$. In the case of the energy density or the pressure these actions lead to a strong reduction of cut-off effects in the high temperature limit [48]. In Sec. 5.1 we will present our numerical data of the electric screening masses. They remain, however, unchanged within statistical errors under an improvement of the action. This suggests that the improvement of the ultraviolet sector does not influence the screening masses much. This may be taken as an indication for the dominance of non-perturbative contributions to m_e.

Using the pole mass definition (2.5), the leading correction to (2.24) can be calculated in one-loop resummed perturbation theory. Based on the assumption that the

infrared limit of the transverse gluon propagator is finite, $-\frac{1}{2}\Pi_{ii}(\vec{p} \to 0, p_4 = 0) = m_m^2 \sim g^4 T^2$, one obtains the gauge invariant result [9, 10]

$$m_e^2(T) = m_{e,0}^2 \left(1 + \frac{\sqrt{6}}{2\pi} g(T) \frac{m_e}{m_{e,0}} \left[\log \frac{2\,m_e}{m_m} - \frac{1}{2} \right] + \mathcal{O}(g^2) \right) \quad . \tag{2.26}$$

As the magnetic mass appearing here is expected to be of $\mathcal{O}(g^2 T)$, the next-to-leading order correction is $\mathcal{O}(g \ln g)$.

2.3.2 The W-Mass in the SU(2)-Gauge-Higgs Model

In the symmetric phase of the SU(2)-gauge-Higgs model the vacuum expectation value of the Higgs field vanishes, $v = 0$. As a consequence, the tree-level mass of the W-boson, $m_{W,0}^2 = \frac{g^2}{4} v^2$, is also zero. On the other hand it is generally believed that in the symmetric phase a W-boson mass of the order $\mathcal{O}(g^2 T)$ is generated non-perturbatively.

A solution to this problem was proposed in [28] for the effective 3-dimensional model. The starting point is a coupled set of gap equations for the W-boson mass and the Higgs boson mass,

$$m_{W,0}^2 = m_W^2 - \delta m_W^2 \quad , \quad m_{H,0}^2 = m_H^2 - \delta m_H^2 \quad . \tag{2.27}$$

m_W and m_H are the masses that enter the propagators of the loop expansion, δm_W^2 and δm_H^2 are treated perturbatively as counter terms, and $m_{W,0}$ and $m_{H,0}$ are the tree-level masses given in (4.2).

Using resummed PT at one-loop order, the authors in [28] derive from (2.27) for Landau gauge the following set of equations:

$$v(\mu^2 + \lambda_3 v^2) = \frac{3}{16\pi} g_3 \left(4\,m_W^2 + \frac{m_H^3}{m_W} \right) \quad , \tag{2.28}$$

$$m_W^2 = \frac{g_3^2}{4} v^2 + m_W\, g_3^2 f(z) \quad , \tag{2.29}$$

$$m_H^2 = \mu^2 + 3\lambda_3 v^2 + m_H\, g_3^2 F(z) \quad , \tag{2.30}$$

with $z = m_W / m_H$. The functions f and F are defined by

$$f(z) \equiv \frac{1}{\pi} \left[\frac{63}{64} \ln 3 - \frac{1}{8} + \frac{1}{32\,z^3} - \frac{1}{32\,z^2} - \frac{1}{16\,z} \right.$$
$$\left. - \left(\frac{1}{64\,z^4} - \frac{1}{16\,z^2} + \frac{1}{8} \right) \ln(1 + 2z) \right] \quad , \tag{2.31}$$

$$F(z) \equiv \frac{1}{\pi} \left[-\left(\frac{3}{32} + \frac{9}{64} \ln 3 \right) \frac{1}{z^2} + \frac{3}{16\,z} - \frac{3}{8} z \right.$$
$$\left. - \left(\frac{3}{8} z^2 - \frac{3}{16} + \frac{3}{64\,z^2} \right) \ln \frac{2\,z + 1}{2\,z - 1} \right] \quad . \tag{2.32}$$

Based on the parameterization of the lattice action used in [28], the relation between the renormalized mass parameter μ and the so-called hopping parameter κ (see Chap. 4) is given by the following two-loop relation [49, 40],

$$
\frac{\mu^2}{g_3^4} = \frac{\beta_3^2}{8}\left(\frac{1}{2\kappa} - 3 + \Sigma(L)\frac{3}{\beta_3}\left(1+\frac{4\lambda_3}{g_3^2}\right)\right)
$$
$$
+ \frac{1}{16\pi^2}\left[\left(\frac{51}{16}+\frac{9\lambda_3}{g_3^2}-12\left(\frac{\lambda_3}{g_3^2}\right)^2\right)\left(\ln\frac{3\beta_3}{2}+0.09\right)+5.0+5.2\frac{\lambda_3}{g_3^2}\right] . \quad (2.33)
$$

$\Sigma(L)$ is a geometrical factor which depends slightly on the size of the lattice,

$$
\Sigma(N_1, N_2, N_3) = \frac{1}{4N_1 N_2 N_3}\sum_{n_i=0}^{N_i-1}{}'\left(\sin^2\frac{\pi n_1}{N_1}+\sin^2\frac{\pi n_2}{N_2}+\sin^2\frac{\pi n_3}{N_3}\right)^{-1} . \quad (2.34)
$$

The prime at the sum indicates that the $n_1 = n_2 = n_3 = 0$ point should be left out. For example, Eq. (2.34) yields for a lattice with infinite volume $\Sigma(\infty) = 0.252731$.

One can now solve the coupled set of equations (2.28) - (2.30) numerically to determine v/g_3, m_W/g_3^2 and m_H/g_3^2 as functions of μ^2/g_3^4 or, under consideration of Eq. (2.33), as functions of κ. We have performed this analysis and discuss the result in Sec. 5.2 where we compare it with the data that we have obtained from our numerical simulation.

Chapter 3

Pure SU(2) Gauge Theory

A Monte Carlo investigation of screening masses in full QCD is extremely time consuming. As one has to extract the masses from the exponential decay of correlation functions at large spatial distance, lattices with a typical extend of $N_s \geq 32$ are needed. To save computer time, it is possible to investigate the theory of strong interaction in a first approximation without taking dynamical quarks into account. In this case one is dealing with pure $SU(N_c)$ gauge theory.

The second simplification step is to reduce the number of colours from $N_c = 3$ to 2. This accelerates a numerical investigation a lot. Both the update of the gauge field and the gauge fixing algorithm need much less CPU time in this case. However, the cost of performing calculations only in pure SU(2) lattice gauge theory are the results themselves. Strictly spoken, they do not have any physical meaning. But SU(2) possesses, as the smallest, non-abelian, unitary group, qualitatively the same properties as SU(3), i.e. asymptotic freedom and confinement. Therefore SU(2) studies are very important to get a quick insight into complex structures of strong interactions. It is, of course, important to try to reproduce qualitatively results obtained from SU(2) gauge theory afterwards also in SU(3) gauge theory.

But SU(2) gauge theory is not only a very simple model for studies concerning the strong interaction. It can also be seen as a limiting case of the SU(2)-gauge-Higgs model which will be introduced in the next chapter. Tuning the hopping parameter towards zero, $\kappa \to 0$, the gauge and the Higgs fields decouple. Therefore the corresponding action describes two independent fields, i.e. the gauge field and the Φ-field. In fact, we have used this feature in Sec. 5.2 where we compare the W-boson screening mass at $\kappa < \kappa_c$ with the magnetic screening mass from SU(2) gauge theory.

A lattice investigation of SU(2) gauge theory first of all requires a lattice regularized version of the continuum action. In general the Wilson action is used which is presented in the next section. To get some control over discretization errors one can in addition perform calculation with so-called improved actions. One of them, a tree-level Symanzik improved action, is also listed. As we are interested in the temperature behaviour of the screening masses we need to have a precise determination of the connection between the gauge coupling and the temperature. This is provided in Sec. 3.2. In the last section of this chapter we finally discuss the deconfinement phase transition.

3.1   Wilson and Symanzik Improved Actions

The naive discretization of the continuum action of pure SU(2) gauge theory gives the Wilson action,

$$S_W = \frac{\beta}{2} \sum_{1 \times 1} \mathrm{Tr}\, U_{1 \times 1} \quad \text{with} \quad \beta = \frac{4}{g^2} \quad , \tag{3.1}$$

where the sum runs over all elementary 1×1 plaquettes $U_{1 \times 1}$, see Fig. 3.1. As

$$U_{1 \times 1} \qquad\qquad\qquad U_{1 \times 2}$$
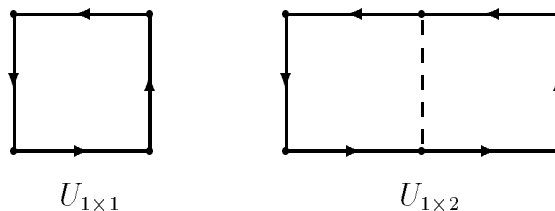
Figure 3.1: The plaquette and the 1×2 Wilson loop.

already mentioned in the introduction to this chapter, we have also used a tree-level Symanzik improved action in order to get some control over the influence of discretization errors caused by the finite lattice spacing a. A possibility to remove systematic $\mathcal{O}(a^2)$ errors in the lattice Wilson action is to replace (3.1) with

$$S_I = \frac{\beta}{2} \left(\frac{5}{3} \sum_{1 \times 1} \mathrm{Tr}\, U_{1 \times 1} - \frac{1}{12} \sum_{1 \times 2} \mathrm{Tr}\, U_{1 \times 2} \right) \quad . \tag{3.2}$$

The second sum now runs over all planar 1×2 Wilson loops $U_{1 \times 2}$. To distinguish the couplings we will denote in the following the Wilson action coupling by β_W and the coupling for the Symanzik improved case by β_I.

With these actions we now have two tools at hand to analyse cut-off dependences of our results. The first method is to use only one action and perform simulations on lattices with different sizes. In this work, for example, we present Wilson action data from lattices of size $32^2 \times 64 \times 8$ and $32^3 \times 4$. For the second method one has to work with a fixed lattice size and compare the results obtained from the different actions. To realize this idea, we simulated the Symanzik improved action also on the $N_\tau = 4$ lattice.

In order to quantify the influence of the non-zero cut-off at finite temperature one should, of course, compare calculations at the same physical temperature, $T \equiv 1/(N_\tau a)$. Furthermore, an accurate determination of the temperature scale is needed for analyzing observables that are expected to depend on a running coupling, $g(T)$, like the screening masses. We thus present in the following section the determination of temperature scales for both actions.

3.2 Determination of the Temperature Scale

The problem to relate the temperature T to the coupling β is equivalent to the task of finding the dependence of the lattice spacing a on the bare coupling g^2. We follow here the approach outlined in [50]. In order to take into account the violations of asymptotic scaling in the coupling regime of interest, we use the general ansatz

$$a \, \Lambda_L \;=\; R(g^2) \cdot \lambda(g^2) \quad \text{with} \tag{3.3}$$

$$R(g^2) \;=\; \exp\left[-\frac{b_1}{2\,b_0^2} \ln(b_0 g^2) - \frac{1}{2\,b_0 g^2} \right] \quad , \tag{3.4}$$

$$b_0 = \frac{11 N_c}{48\,\pi^2} \quad , \quad b_1 = \frac{34}{3} \left(\frac{N_c}{16\,\pi^2} \right)^2 \quad . \tag{3.5}$$

The function $\lambda(g^2)$ parameterizes the asymptotic scaling violations. For this we use an exponential ansatz

$$\lambda(g^2) = \exp\left[\frac{1}{2\,b_0^2} \left(d_1 g^2 + d_2 g^4 + d_3 g^6 + \dots \right) \right] \quad . \tag{3.6}$$

Using $T = 1/(N_\tau a)$ we obtain from Eq. (3.3)

$$\frac{1}{N_\tau R(g_c^2)} = \lambda(g_c^2) \frac{T_c}{\Lambda_L} \quad . \tag{3.7}$$

Here g_c^2 is the value of the bare coupling at the critical temperature T_c of the deconfinement phase transition at given N_τ. Using results for $g_c^2(N_\tau)$ [51, 52] the function $\lambda(g_c^2)$ is obtained from a fit where T_c/Λ_L is an additional free parameter.

Based on the Wilson action data for g_c^2 summarized in [51], the best fit in [50] is given by the parameterization $d_1 = d_2 = d_{n>3} = 0$. Their fit results are $d_3 = 5.529(63) \cdot 10^{\perp 4}$ and $(T_c/\Lambda_L)_W = 21.45(14)$.

For the Symanzik improved action we have performed a similar fit, using the critical couplings computed in [52] for $N_\tau \geq 4$. Our best parameterization is given by $d_1 = d_{n>2} = 0$, and our fit results are $d_2 = 5.12(18) \cdot 10^{\perp 4}$ and $(T_c/\Lambda_L)_I = 4.94(11)$. The fit can also be seen in Fig. 3.2.
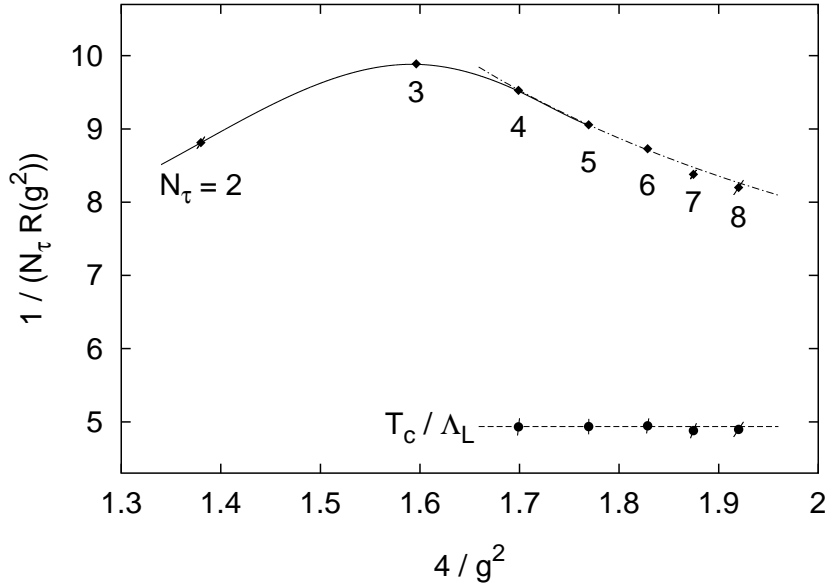
Figure 3.2: The critical temperature $1/(N_\tau R(g^2))$ vs. $4/g^2$ for $N_\tau = 2, \ldots, 8$. The data for $g_c^{\perp 2}(N_\tau)$ are taken from [52]. The solid line is a spline interpolation of the data, the dashed-dotted line is obtained from a fit for $N_\tau \geq 4$.

For the ratios of Λ-parameter we use the perturbatively calculated values, i.e. $\Lambda_{L,I}/\Lambda_{L,W} = 4.13089(1)$ [53] and $\Lambda_{\overline{MS}}/\Lambda_{L,W} = 19.82314$ [54]. Then we find for the critical temperature a result which, within 5%, coincides with the previously determined continuum extrapolation for the Wilson action

$$\frac{T_c}{\Lambda_{\overline{MS}}} = \begin{cases} 1.08 \pm 0.01 & \text{standard Wilson action [50]} \\ 1.03 \pm 0.03 & \text{tree-level improved (1,2)-action} \end{cases} . \quad (3.8)$$

In the following, we will use an averaged value of $T_c/\Lambda_{\overline{MS}} = 1.06$.

We finally need to extract the temperature in units of the critical temperature at given N_τ. This is given by

$$\frac{T}{T_c} = \frac{R(g_c^2) \cdot \lambda(g_c^2)}{R(g^2) \cdot \lambda(g^2)} \quad . \quad (3.9)$$

Using Eq. (3.9), the fit results for λ and the critical couplings from [51, 52], we can now relate the temperature T to the coupling $\beta = 4/g^2$. The results for the couplings used in our analysis are listed in Tab. 3.1. The good agreement found

$N_\tau = 4$		$N_\tau = 8$		$N_\tau = 4$	
β_W	T/T_c	β_W	T/T_c	β_I	T/T_c
2.512	2.004	2.74	2.007	1.92	1.984
2.643	3.002	2.88	3.031	2.063	3.031
2.74	4.013	2.97	3.929	2.152	3.923
2.88	6.062	3.12	6.016	2.30	5.979
2.955	7.527	3.20	7.530	2.382	7.528
3.023	9.143	3.27	9.151	2.452	9.149
3.219	15.88	3.47	15.89	2.652	15.88
3.743	66.78	4.00	66.71	3.183	66.68
4.24	253.5	4.50	253.3	3.684	253.2
4.738	953.1	5.00	953.9	4.185	954.0
5.238	3581	5.50	3578	4.685	3572
5.737	13383	6.00	13401	5.186	13393

Table 3.1: Relations between the couplings and the temperatures.

from this analysis for $T_c/\Lambda_{\overline{MS}}$ calculated with two different actions suggests that our temperature scale is of similar accuracy.

3.3 The Deconfinement Phase Transition

One of the characteristic features of QCD is the deconfinement phase transition. Below a critical temperature T_c quarks and gluons can only exist in colourless, bounded states. This situation changes dramatically in the high temperature range (and/or at very high pressure). In this phase one expects the existence of a quark gluon plasma (see for example [55]). This is a medium in which both quarks and gluons behave like free, unbounded particles. It is known for a long time that pure $SU(N_c)$ gauge theory also possesses this phase transition. Studies of the heavy quark potential, using Polyakov Loop correlation functions, have shown that quarks are asymptotic free (at small distances) and confined (at large separations) below T_c, whereas they decouple above T_c, see Eq. (2.8). The order of the phase transition was also investigated in much detail. In [56] it was proposed that the phase transition of pure $SU(N_c)$ gauge theory lies in the same universality class as the corresponding transitions of Z_{N_c} spin systems of the same spatial dimension. Therefore the deconfinement phase transition is of second order for pure $SU(2)$ gauge theory [57] (as for

the Ising model) and of first order for $N_c = 3$ [58, 59] (as for the three-state Potts model). In the case of $N_c = 2$ the critical exponents were verified up to very high accuracy in [60]. Within errors, they coincide with the corresponding exponents from the 3-dimensional Ising model [61].

The order parameter of the deconfinement phase transition is the Polyakov loop,

$$L(\vec{x}) \equiv \prod_{x_4=1}^{N_\tau} U_4(\vec{x}, x_4) \quad . \tag{3.10}$$

Let us consider the following global $Z(N_c)$ rotation of all time like link variables at fixed x_4,

$$U_4(\vec{x}, x_4) \rightarrow U_4'(\vec{x}, x_4) = z\, U_4(\vec{x}, x_4) \quad \text{with} \quad z \in Z(N_c) \quad . \tag{3.11}$$

Whereas the actions (3.1) and (3.2) are invariant under the transformation (3.11), the Polyakov loop is not,

$$L(\vec{x}) \rightarrow z\, L(\vec{x}) \quad . \tag{3.12}$$

Therefore the expectation value of the averaged Polyakov loop,

$$\langle L \rangle = \frac{1}{N_s^3} \frac{1}{N_c} \left\langle \sum_{\vec{n}} \text{Tr}\; L(\vec{n}) \right\rangle \quad , \tag{3.13}$$

vanishes in the phase with the global $Z(N_c)$ symmetry and acquires a finite value in the symmetry broken phase,

$$\langle L \rangle \;=\; 0 \quad \text{for } T < T_c \quad , \tag{3.14}$$

$$\langle L \rangle \;\neq\; 0 \quad \text{for } T > T_c \quad . \tag{3.15}$$

It was shown in [43] that $\langle L \rangle = 0$ corresponds to a system with an isolated quark with infinite free energy. Therefore the phase with $\langle L \rangle = 0$ describes confinement. On the other hand, the isolated quark system is of finite free energy at $\langle L \rangle \neq 0$, i.e. in the deconfinement phase.

Chapter 4

The SU(2)-Gauge-Higgs Model

4.1   The 4-dimensional Model

The electroweak sector of the SM is described by a SU(2)⊗U(1) gauge theory. Let us denote the coupling of the SU(2) gauge field by g and the one of the U(1) gauge field by g', respectively. The relation between both couplings is given by the Weinberg angle, $g'/g = \tan\theta$. By experiment, θ is known to be relatively small, $\sin^2\theta \simeq 0.23$. Therefore one can neglect in a first approximation the contribution of the U(1) gauge field.

Furthermore, the quarks and leptons are coupled very weakly to the Higgs field, with the top quark coupling being a possible exception. As a consequence, one can also neglect the contribution of dynamical fermions.

Both simplifications result in the SU(2)-gauge-Higgs model [4]. It describes the interaction of a complex scalar doublet field with the SU(2) gauge field and is a quite good approximation to the electroweak sector of the SM.

We present now the lattice discretized action of the SU(2)-gauge-Higgs model, which is originally formulated in three space and one time dimension:

$$S^{4d} = \frac{\beta}{2} \sum_{1\times1} \mathrm{Tr}\, U_{1\times1} + \frac{1}{2} \sum_x \sum_{\mu=1}^{4} \mathrm{Tr}\, \Phi^\dagger(x) U_\mu(x) \Phi(x+\hat{\mu})$$

$$- \frac{1}{2\kappa} \sum_x \frac{1}{2} \mathrm{Tr}\, \Phi^\dagger(x) \Phi(x) - \frac{\lambda}{4} \sum_x \left(\frac{1}{2} \mathrm{Tr}\, \Phi^\dagger(x)\Phi(x) \right)^2 \quad . \qquad (4.1)$$

As in the case of pure gauge theory, $\beta = 4/g^2$ denotes the coupling of the SU(2) gauge field. It should, however, not be confused with the coupling used in Eq. (3.1). $U_{1\times1}$ is again an elementary plaquette, and $\Phi(x)$ describes the complex Higgs doublet

according to Eq. (2.15). The coupling κ is the hopping parameter. The quartic coupling λ is related to the $T = 0$ tree-level masses of the Higgs boson $(m_{H,0})$ and of the W-bosons $(m_{W,0})$ by

$$\lambda = \frac{1}{8} \frac{m_{H,0}^2}{m_{W,0}^2} g^2 \quad \text{with} \quad m_{H,0}^2 = 2\lambda v^2 \quad \text{and} \quad m_{W,0}^2 = \frac{g^2}{4} v^2 \quad . \tag{4.2}$$

At this point, the most straightforward way would be to perform calculations using the action (4.1). But this is not without problems [62]. As the 4d theory is not super-renormalizable it contains ultraviolet divergences in any order of PT. Therefore the scaling behaviour, which is needed to relate the lattice and the continuum parameters, becomes quite complicated. This problem disappears in the dimensional reduced 3d theory. Because of its super-renormalizable property only one- and two-loop graphs are divergent.

In addition, the dimensional reduced theory has another advantage over the 4d theory. After integrating out the heavy modes, i.e. the A_0 field, the 3d theory contains only one essential mass or energy scale, $m_Q \sim g^2 T$. On the other hand, the unreduced theory contains two additional mass scales, the temperature T and the Debye (or electric) screening mass $m_D \sim gT$.

4.2   Dimensional Reduction and the Effective 3-dimensional Model

In this section we will briefly outline the idea of dimensional reduction within the SU(2)-gauge-Higgs model and quote the most important results. For a detailed discussion of this topic we refer to [62, 63, 64] and references therein.

The electroweak theory in the parameter space of interest is characterized by a weak coupling, $g^2 \ll 1$. Therefore the theory involves several mass scales,

$$T \;\gg\; m_D \sim gT \;\gg\; m_Q \sim g^2 T \quad . \tag{4.3}$$

As we are interested in infrared physics, the mass scale $m_Q \sim g^2 T$ plays a dominant role.

The next thing one has to take into account is the Euclidean path integral formulation of the field theory. Let us start with the continuum expression of the bosonic[1]

---

[1] As we are dealing only with bosonic fields we will neglect anti-periodic fermionic fields in the discussion. Of course, dimensional reduction works also in this case.

partition function

$$\mathcal{Z} = \int_{per} \mathcal{D}A_\mu \mathcal{D}\Phi \mathcal{D}\Phi^\dagger \; \exp\left\{-S[A_\mu, \Phi, \Phi^\dagger]\right\} \tag{4.4}$$

with periodic boundary conditions

$$A_\mu(\vec{x}, 0) = A_\mu(\vec{x}, 1/T) \; , \quad \Phi(\vec{x}, 0) = \Phi(\vec{x}, 1/T) \quad . \tag{4.5}$$

The action is given by an integral over the Lagrange density,

$$S[A_\mu, \Phi, \Phi^\dagger] = \int_0^{\frac{1}{T}} \mathrm{d}\tau \int_V \mathrm{d}\vec{x} \; \mathcal{L}(A_\mu, \Phi, \Phi^\dagger) \quad . \tag{4.6}$$

From expression (4.6) one can see that at very high temperature the length of the τ-integration becomes very narrow. For the lattice regularized version of (4.6) this has the consequence that the extend of the τ-direction of the lattice is small. This suggests that the important features of the theory might be described by an effective theory in three dimensions.

Due to the finite length of the τ-integration and the condition (4.5), the fields can be expanded in Fourier series. The propagators of the Fourier or Matsubara modes are of the form $[\vec{k}^2 + m_0^2 + (2n\pi T)^2]^{\perp 1}$, which means that the non-static modes ($n = \pm 1, \pm 2, \ldots$) acquire a mass $2n\pi T$. Because of relation (4.3) these masses are heavy compared to the infrared mass scale m_Q. As a consequence, they can be integrated out perturbatively, using $m_Q/(\pi T)$ as an expansion parameter.

At this point, the preliminary result is an effective 3-dimensional theory which consists of the SU(2) gauge field, the fundamental Higgs field and an adjoint Higgs field. The latter is the remnant of the temporal component of the 4-dimensional gauge field and has a mass $\sim gT$. As this is larger than the infrared mass scale m_Q, it can also be integrated out perturbatively. The remaining result is an action which is very similar to its 4-dimensional counterpart (4.1). Of course, the sum over the directions is now restricted to the three spatial directions. The effective 3-dimensional action is

$$S^{3d} = \frac{\beta_3}{2} \sum_{1 \times 1} \mathrm{Tr}\, U_{1 \times 1} + \frac{1}{2} \sum_x \sum_{i=1}^3 \mathrm{Tr}\, \Phi^\dagger(x) U_i(x) \Phi(x + \hat{\imath})$$
$$- \frac{1}{2\kappa} \sum_x \frac{1}{2}\mathrm{Tr}\, \Phi^\dagger(x)\Phi(x) - \frac{\lambda_3}{4} \sum_x \left(\frac{1}{2}\mathrm{Tr}\, \Phi^\dagger(x)\Phi(x)\right)^2 \quad . \tag{4.7}$$

The relation of the three dimensionless lattice couplings β_3, λ_3 and κ to the couplings of the original $T = 0$, SU(2)-gauge-Higgs model is given by the following sequence of equations [16]:

$$\beta_3 = \frac{4}{g_3^2 \Theta} \quad , \quad g_3^2 = g^2 \left(1 - \frac{g}{20\pi}\sqrt{\frac{5}{6}}\right) \quad , \tag{4.8}$$

$$\lambda_3 \;=\; \left(\lambda - \frac{9}{320\pi} \sqrt{\frac{5}{6}}\, g^3 \right) \Theta \quad , \tag{4.9}$$

$$\frac{1}{\kappa} \;=\; m^2 a^2 + 6 \tag{4.10}$$

$$+ \left(\frac{3}{16} g^2 + \frac{1}{2}\lambda - \frac{3g^3}{16\pi}\sqrt{\frac{5}{6}} \right) \Theta^2 - \Theta\,\Sigma(L) \left(\frac{3}{2} g^2 + 6\lambda - \frac{15\,g^3}{32\pi}\sqrt{\frac{5}{6}} \right) \quad .$$

We remark that Eq. (4.10) is based on our parameterization of the lattice action, Eq. (4.7). It corresponds to relation (2.33) for the parameterization used in [28]. m represents the renormalized mass parameter of the original theory. The parameter $\Theta \equiv aT$ controls the temperature dependence and involves the lattice spacing which has to be chosen appropriately. One expects that $\Theta \simeq 1$ works fine.

To summarize, the set of equations (4.7) - (2.34) presents a powerful tool to perform non-perturbative lattice calculations of the effective 3-dimensional SU(2)-gauge-Higgs model. They both give the action which has to be simulated and tell how to relate the results to the original, 4-dimensional $T = 0$ theory.

4.3   The Electroweak Phase Transition

One of the main features of the electroweak sector of the standard model is the occurrence of the electroweak phase transition. In the low temperature phase ($\kappa > \kappa_c$) one has an infinite number of states with absolute minima in the potential which are all lying on a circle. By choosing one particular state as the ground state one explicitly breaks this rotational symmetry (Higgs mechanism). At high temperatures ($\kappa < \kappa_c$) the situation changes. The potential now has only one absolute minimum and therefore the symmetry is restored.

The strength of this phase transition strongly depends on the couplings β and λ. Let us assume a fixed value of β which resembles continuum physics, i.e. $\beta = \mathcal{O}(10)$. Then the phase transition is of first order for small values of λ. This is indicated in Fig. 4.1 by the solid line. It seperates the Higgs phase, in which the electroweak symmetry is broken ($\kappa > \kappa_c$ resp. $T < T_c$), from the confinement phase ($\kappa < \kappa_c$ resp. $T > T_c$). The strength of the first order nature decreases with increasing λ. At a particular λ_c the phase transition becomes too weak and we are left with a crossover, the filled circle in Fig. 4.1 and the region to its right. We note that, using relation (4.2), the critical λ-parameter can be transformed into a critical value of the $T = 0$ Higgs mass, $m_{H,c}$. Whereas the critical line can not be calculated analytically, the situation is different at $\lambda = 0$. Here the system has a Gaussian fixed point, and the critical hopping parameter is $1/(2\,\kappa_c) = 2\,d$.
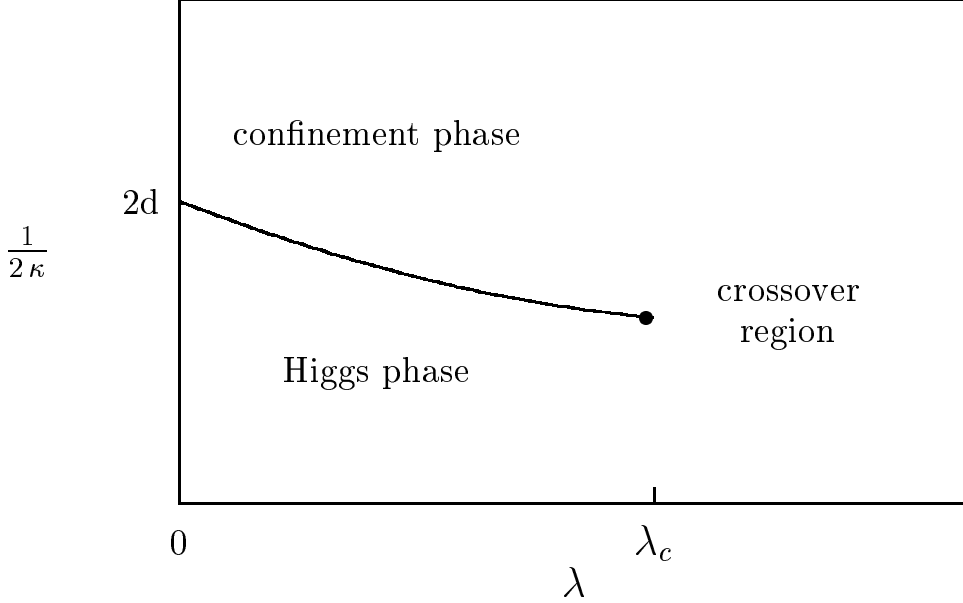
Figure 4.1: The phase structure of the d-dimensional SU(2)-gauge-Higgs model at $\beta = \mathcal{O}(10)$.

For a better understanding of the SU(2)-gauge-Higgs model it is necessary to determine λ_c. The "classical" methods are, for example, to calculate the Φ^2-susceptibility or the so-called Binder-cumulants. All these methods start in the phase with small λ and determine if the phase transition is still of first order at the λ under consideration. However, these ansätze become unreliable in the region of interest, i.e. close to λ_c.

In this work we prefer an alternative way that investigates the theory in the crossover region, i.e. at large values of λ resp. of λ_3 in the case of three dimensions. As the critical Higgs mass was roughly known to be $m_{H,c} \simeq 70 - 80$ GeV, we have investigated the SU(2)-gauge-Higgs model at $\lambda_3 = 0.0485458, 0.0523100, 0.0668478$ and 0.0830965. Assuming a zero temperature W-mass of $m_W = 80.6$ GeV, these values correspond to $m_H \simeq 77$ GeV, 80 GeV, 90 GeV and 100 GeV. In addition, we have also performed one simulation at a value of λ_3 which is known to lie in regime where the phase transition is strongly of first order, $\lambda_3 = 0.0283650$, corresponding to $m_H \simeq 60$ GeV. We will now present the method that we have used to determine $\lambda_{3,c}$. The idea is to continue the partition function $\mathcal{Z}$ analytically into the complex plane as a function of the complex hopping parameter κ. Then one analyses the Fisher or Lee-Yang zeros [65] of $\mathcal{Z}$. To get an impression of the behaviour of $\mathcal{Z}$ in the complex κ-plane, we show in Fig. 4.2 lines with $\text{Re}(\mathcal{Z}(\kappa)) = 0$ and $\text{Im}(\mathcal{Z}(\kappa)) = 0$, respectively. The intersections of these lines give, of course, $\mathcal{Z}(\kappa) = 0$.

Let us denote the lowest zero of the partition function $\mathcal{Z}$ with z_0, i.e. $\mathcal{Z}(z_0) = 0$ with
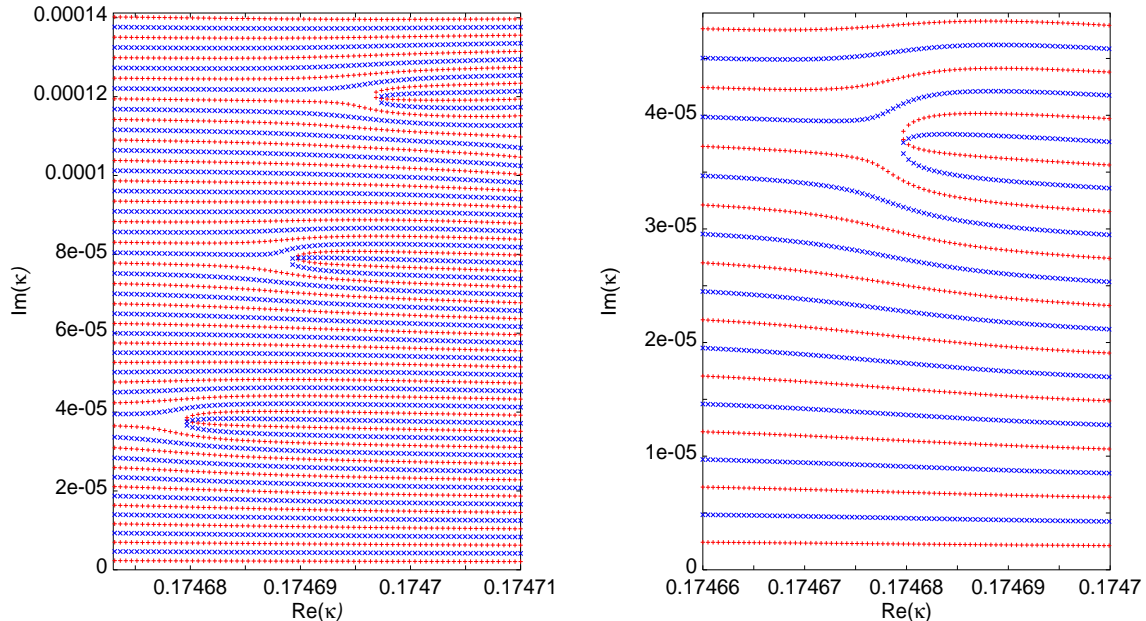
Figure 4.2: Zeros of the partition function at $\lambda_3 = 0.0523100$ on a 32^3 lattice. A '+' refers to $\mathrm{Re}(\mathcal{Z}(\kappa)) = 0$, a 'x' refers to $\mathrm{Im}(\mathcal{Z}(\kappa)) = 0$. The right picture is a blowup of the region around the lowest zero of $\mathcal{Z}$.

$|z_0| = \min\{|\kappa| \,; \, \mathcal{Z}(\kappa) = 0 \,, \kappa \text{ complex}\}$. Inspired by the high temperature phase of the Ising model, we expect in the vicinity of the critical end-point the scaling law

$$\mathrm{Im}(z_0) = C\, N_s^{\perp 1/\tilde{\nu}} + R(\lambda_3) \quad . \tag{4.11}$$

Eq. (4.11) is based on the fact that for a first order phase transition the lowest zero z_0 must be completely real in the thermodynamic limit. For this case one therefore needs $R = 0$. On the other hand, $R > 0$ indicates that, at a given λ_3, the system has only a crossover.

Our strategy to localize the end-point is to determine the value of λ_3 at which the regular contribution R to the scaling law vanishes, $R(\lambda_{3,c}) = 0$. In Tab. 4.1 and Fig. 4.3 we display $\mathrm{Im}(z_0)$ vs. N_s for various values of λ_3. The dashed line in Fig. 4.3 has the parameters $\tilde{\nu} = 1/3$ and $R = 0$, corresponding to a first order phase transition. As expected, the data at $\lambda_3 = 0.0283650$ are consistent with this curve.

The solid curves in Fig. 4.3 represent fits in the regime of interest, $\lambda_3 \geq 0.0485458$, with the scaling law (4.11). For these fits we assume an universal exponent $\tilde{\nu}$ for all four values of λ_3. From a fit over all datasets we obtain $\tilde{\nu} = 0.417(6)$ with $\chi^2/\mathrm{dof} = 0.76$. The fit results for the regular parts are listet in Tab. 4.2. As expected, they increase with increasing λ_3. This behaviour can also be seen in Fig. 4.4 in which the constant R is displayed as function of λ_3. The data are consistent with a linear

	$\lambda_3 =$				
	0.0283650	0.0485458	0.0523100	0.0668478	0.0830965
N_s	$\mathrm{Im}(z_0)/10^{\perp 4}$	$\mathrm{Im}(z_0)/10^{\perp 4}$	$\mathrm{Im}(z_0)/10^{\perp 4}$	$\mathrm{Im}(z_0)/10^{\perp 4}$	$\mathrm{Im}(z_0)/10^{\perp 4}$
8	4.390(52)	–	–	–	–
10	2.691(27)	–	–	–	–
12	1.774(40)	–	–	–	–
16	0.787(11)	1.598(8)	1.744(17)	2.298(30)	2.874(38)
20	0.426(4)	0.937(20)	1.033(10)	1.418(16)	1.906(30)
22	–	–	–	–	1.602(51)
24	–	0.617(11)	0.712(13)	1.030(21)	–
28	–	0.430(8)	0.496(11)	0.784(16)	1.086(30)
32	–	0.309(4)	0.377(7)	0.668(26)	0.940(22)
36	–	0.240(8)	0.296(9)	–	–
40	–	0.192(4)	0.248(12)	0.442(24)	0.811(101)
48	–	0.124(7)	0.172(9)	0.414(61)	0.565(67)

Table 4.1: Imaginary parts of the lowest zeroes of the partition function.

λ_3	R
0.0485458	$0.97(84) \cdot 10^{\perp 6}$
0.0523100	$0.56(9) \cdot 10^{\perp 5}$
0.0668478	$0.25(2) \cdot 10^{\perp 4}$
0.0830965	$0.47(3) \cdot 10^{\perp 4}$

Table 4.2: Regular parts of the fit results acc. to (4.11).

dependence on λ_3 and the fit results into $\lambda_{3,c} = 0.04795(52)$ which corresponds to a critical Higgs-mass of approximately $m_{H,c} = 75.7(4)$ GeV. We note that this value is slightly shifted by a very recent investigation [18]. The authors obtain there as a preliminary result $\lambda_{3,c} = 0.04812(12)$ and $m_{H,c} = 75.8(1)$ GeV, respectively.
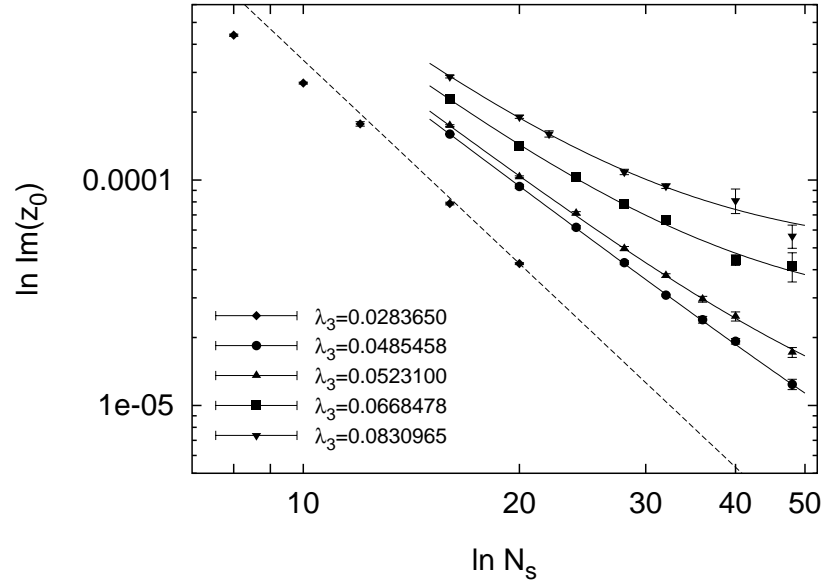
Figure 4.3: Imaginary parts of the lowest zeroes of the partition function.
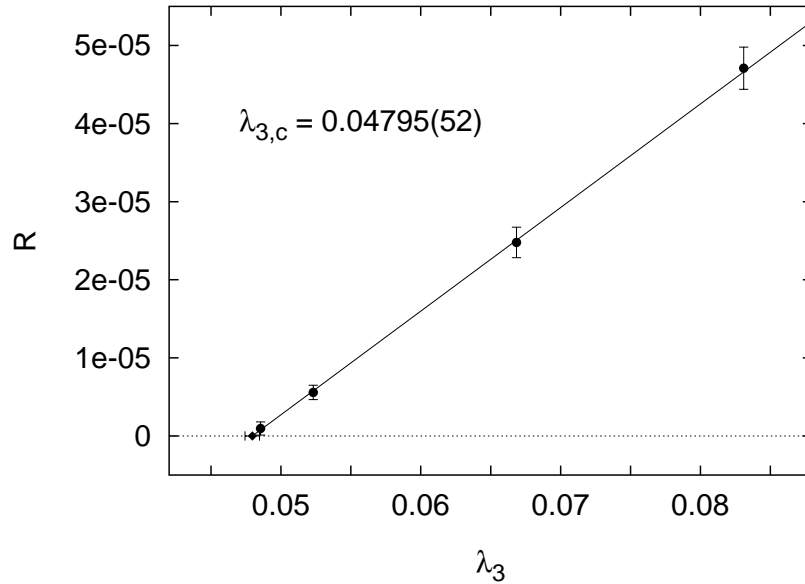
Figure 4.4: The determination of $\lambda_{3,c}$.

Chapter 5

Screening Masses - Numerical Results

5.1 Gluon Screening Masses in Pure SU(2) Gauge Theory

5.1.1 Screening Masses from the Gluon Propagator

In [20] we performed a first analysis of the behaviour of the electric and magnetic screening masses in Landau gauge. The results are summarized in [21] and [22]. Whereas in these works we had calculated the gluon propagator only at vanishing momentum, we extended the analysis in [15] to finite momenta. Furthermore we used in [13]-[15] temperatures very much higher than in [20]-[22] in order to possibly get in closer contact with perturbation theory. Finally, we used in addition to the Wilson action in [13]-[15] also the in Sec. 3.1 introduced tree-level Symanzik improved action. In this section we summarize the results from [13]-[15].

In Sec. 2.2.1 we have given the relations between the energies in the electric and magnetic sectors and gluonic correlation functions, Eqs. (2.3) and (2.4). To extract the screening masses we use the dispersion relation between energy, screening mass and momentum, which on the lattice has the form

$$\sinh^2 \frac{aE_i}{2} = \sinh^2 \frac{am_i}{2} + \alpha \sum_{j=1}^{3} \sin^2 \frac{ap_j}{2} \quad , \quad i = e, m \quad . \tag{5.1}$$

In (5.1) we have introduced a factor α which parameterizes deviations from a free particle dispersion relation ($\alpha \equiv 1$) introduced by a thermal medium.

Using $T = 1/(N_\tau a)$ we can now compute the screening masses in units of the temperature, m_i/T with $i = e$, m. We have performed simulations using the Wilson action on lattices of sizes $32^3 \times 4$ and $32^2 \times 64 \times 8$ and using the tree-level Symanzik improved action on a $32^3 \times 4$ lattice. At each value of the gauge coupling we performed measurements on at least 1000 configurations, see Tab. 5.1. Two consecutive config-

$32^3 \times 4$		$32^2 \times 64 \times 8$		$32^3 \times 4$	
β_W	# meas.	β_W	# meas.	β_I	# meas.
2.512	2000	2.74	1220	1.92	2000
2.643	2000	2.88	1000	2.063	2000
2.74	2000	2.97	1000	2.152	2000
2.88	2000	3.12	1000	2.30	2000
2.955	2000	3.20	1000	2.382	2000
3.023	2000	3.27	1440	2.452	2000
3.219	2000	3.47	1140	2.652	2000
3.743	2000	4.00	1000	3.183	2000
4.24	2000	4.50	1160	3.684	2000
4.738	2000	5.00	1000	4.185	2000
5.238	2000	5.50	1000	4.685	2000
5.737	2000	6.00	1000	5.186	2000

Table 5.1: Number of measurements (pure SU(2) gauge theory).

urations were separated by at least 10 update iterations, and each update consists of at least four overrelaxation sweeps, followed by one heatbath sweep.

From the exponential decay of the gluon correlation functions G_e and G_m we extract the screening masses. A rather technical problem is the procedure to select a reliable fit range in which $G_e(p_\perp, x_3)$ and $G_m(p_\perp, x_3)$ (see (2.3) and (2.4)) can be fitted to extract the energies in the electric and magnetic sectors. This is described in App. A.1.

The results for the screening masses (from the $\vec{p} = 0$ measurements) and the energies ($\vec{p} \neq 0$) are listed in Tabs. 5.2 and 5.3 respectively.

Zero Momentum Results

Let us first discuss the electric screening mass, extracted from the measurements at vanishing momentum $\vec{p} = 0$. In Fig. 5.1 we show m_e/T for both types of actions and the two different lattices we have used. One can see at once that, within errors, m_e/T does not differ significantly for the three sets. Even the tree-level Symanzik

Wilson action, $32^2 \times 64 \times 8$ lattice					
β_W	$m_e(T)/T$	$m_m(T)/T$	β_W	$m_e(T)/T$	$m_m(T)/T$
2.74	2.39(11)	2.01(29)	3.47	1.62(4)	0.92(7)
2.88	1.95(4)	1.24(4)	4.00	1.62(8)	0.66(3)
2.97	1.91(7)	1.15(4)	4.50	1.55(5)	0.61(2)
3.12	1.92(9)	1.23(14)	5.00	1.41(3)	0.52(3)
3.20	1.92(10)	1.09(10)	5.50	1.27(5)	0.42(2)
3.27	1.93(6)	1.03(5)	6.00	1.26(5)	0.37(2)

Table 5.2: Electric and magnetic screening masses from $G_e(k_1 = 0)$ and $G_m(k_1 = 0)$.

improved action, which cures discretization errors of $\mathcal{O}(a^2)$ in the action, does not shift the electric screening mass in any direction. This makes clear that ultraviolet modes do not contribute significantly to the screening mass. As a consequence, we have analysed all three data sets together.

Fig. 5.1 shows that m_e/T only depends very weakly on the temperature for small values of the coupling β, corresponding to temperatures less than about $10\,T_c$. A constant fit in this temperature range yields $m_e(T)/T = 1.938(15)$. This behaviour is qualitatively similar to what we have observed in [22]. For temperatures $1.3\,T_c < T < 16\,T_c$ we found in [22] $m_e(T)/T = 2.484(52)$. The difference between these values arises from different methods of extracting the screening masses. Whereas in this work we performed correlated fits of the gluon correlation functions over variable fit ranges (see App. A.1), we obtained m_e and m_m in [22] from uncorrelated fits in the fixed range $zT \geq 1$. Our new method results in screening masses which are up to 20% smaller. Since it accounts for possible correlations in the data, the results should be more reliable.

A constant behaviour of m_e/T is also observed in a very recent study of SU(2) gauge theory in the axial gauge. Demanding magnetic stability of the theory, the authors in [66] find in the temperature range from $T = 4\,T_c$ up to $T = 16\,T_c$ approximately $m_e/T \simeq 0.84$. A modification of their perturbative calculation shifts this value slightly higher, $m_e/T \simeq 1.1$. Even if this agrees on a qualitative level with our result, we want to point out that, similar to our first analysis [22], the temperature range under investigation is too narrow in [66] to rule out the expected gT-behaviour of m_e .

In contrast to [22] we have calculated m_e now also at very high temperatures (up to $T \sim 13400\,T_c$; see Tab. 3.1). From this analysis it becomes evident that m_e/T runs with T. Since this is expected from perturbation theory it is meaningful to test whether perturbative predictions also work quantitatively.

Wilson action, $32^3 \times 4$ lattice			
	$E_e(\vec{p}, T)/T$, extracted from		
β_W	$G_e(k_1\!=\!0)$	$G_e(k_1\!=\!1)$	$G_e(k_1\!=\!2)$
2.512	2.14(11)	2.71(18)	2.46(5)
2.643	2.24(9)	2.28(8)	2.34(4)
2.74	1.94(5)	2.13(5)	2.33(7)
2.88	2.03(7)	2.03(4)	2.33(5)
2.955	1.87(4)	1.94(4)	2.27(5)
3.023	2.10(14)	2.12(13)	2.25(4)
3.219	1.80(7)	1.93(5)	2.03(3)
3.743	1.58(3)	1.78(7)	1.94(2)
4.24	1.64(8)	1.55(3)	2.01(4)
4.738	1.33(3)	1.51(4)	1.91(8)
5.238	1.19(2)	1.40(3)	1.83(4)
5.737	1.26(3)	1.35(4)	1.83(4)

Symanzik action, $32^3 \times 4$ lattice			
	$E_e(\vec{p}, T)/T$, extracted from		
β_I	$G_e(k_1\!=\!0)$	$G_e(k_1\!=\!1)$	$G_e(k_1\!=\!2)$
1.92	2.10(6)	2.18(5)	2.36(4)
2.063	1.96(5)	2.17(5)	2.36(4)
2.152	2.08(8)	2.04(5)	2.23(5)
2.30	1.76(3)	1.95(4)	2.91(26)
2.382	2.01(11)	2.00(4)	2.54(9)
2.452	1.70(5)	2.04(9)	2.21(5)
2.652	1.72(6)	1.53(21)	2.05(3)
3.183	1.69(8)	1.61(2)	2.13(11)
3.684	1.44(8)	1.75(6)	1.94(2)
4.185	1.50(6)	1.30(1)	1.85(4)
4.685	1.19(6)	1.45(7)	1.74(2)
5.186	1.31(8)	1.29(4)	1.77(5)

Table 5.3: Energies from the electric sector of gluon correlation functions.
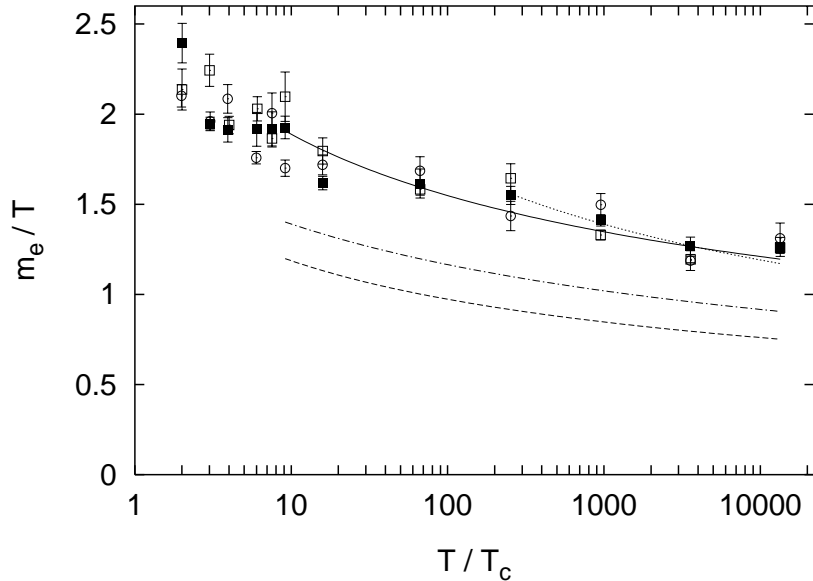
Figure 5.1: Electric screening masses in units of the temperature vs. T/T_c from simulations with Wilson action on $32^2 \times 64 \times 8$ (filled squares) and $32^3 \times 4$ (open squares) lattices and with Symanzik action on a $32^3 \times 4$ lattice (open circles). The dashed line is the tree-level result (2.24), the dashed-dotted line is a self consistent determination of m_e, using (2.26). The other lines are one parameter fits, using ansatz (5.4) (solid line, for $T \geq 9 \, T_c$) and ansatz (5.6) (dotted line, for $T \geq 250 \, T_c$) respectively.

At lowest order perturbation theory for two colour degrees of freedom and without taking dynamical quarks into account, the electric mass is given by the well known relation (2.24). For the running coupling we use the 2-loop formula

$$g^{\perp 2}(T) = \frac{11}{12\pi^2} \ln \frac{\mu}{\Lambda} + \frac{17}{44\pi^2} \ln \left[2 \ln \frac{\mu}{\Lambda} \right] \tag{5.2}$$

with $\mu = 2\pi T$ being the lowest lying Matsubara frequency. Hence

$$g^{\perp 2}(T) = \frac{11}{12\pi^2} \left(\ln \frac{T}{T_c} + \ln \frac{2\pi T_c}{\Lambda} \right) + \frac{17}{44\pi^2} \ln \left[2 \left(\ln \frac{T}{T_c} + \ln \frac{2\pi T_c}{\Lambda} \right) \right] \quad . \tag{5.3}$$

We start the discussion of our data with a comparison with the perturbative result (2.24), which is shown in Fig. 5.1 as a dashed line. The numerical data for m_e are lying about 60% above the lowest order perturbative result (2.24). However, the functional dependence of the electric mass on the temperature seems to be well described by $m_e \sim gT$.

To verify the temperature dependence of the electric mass quantitatively, we have performed several fits of m_e/T vs. $\ln(T/T_c)$ for temperatures $T \geq 9 \, T_c$. In our one

parameter fits we fix the Λ-parameter appearing in the temperature dependent running coupling to $\Lambda_{\overline{\text{MS}}}$ and therefore use the MC-result for $T_c/\Lambda_{\overline{\text{MS}}}$, i.e. $T_c/\Lambda_{\overline{\text{MS}}} = 1.06$ (see page 26). In those cases where we parameterize the screening masses only by its leading g^2-dependence the effect of higher order corrections can be partially taken into account in a modification of the Λ-parameter. We, therefore, also performed two parameter fits with a free ratio $\Lambda_{\text{fit}}/\Lambda_{\overline{\text{MS}}}$.

The first fit ansatz we use is

$$\left(\frac{m_e(T)}{T}\right)^2 = A_{\text{fit}}\, g^2(T) \quad . \tag{5.4}$$

The results obtained with this ansatz are summarized in Tab. 5.4. They again reflect

1-parameter fit		2-parameter fit	
A_{fit}	1.69(2)	A_{fit}	1.92(9)
$\Lambda_{\text{fit}}/\Lambda_{\overline{\text{MS}}}$	1	$\Lambda_{\text{fit}}/\Lambda_{\overline{\text{MS}}}$	0.33(13)
χ^2/dof	4.51	χ^2/dof	4.14

Table 5.4: Fit results of $(m_e(T)/T)^2$, extracted from gluon correlation functions at zero momentum, using the fit ansatz (5.4).

that the lowest order perturbative result (2.24) does not describe the data very well. The fit parameter A_{fit} is much bigger than the theoretical value 2/3. The solid line shown in Fig. 5.1 is the result from the one parameter fit. It shows, as noted above, that at least the variation of m_e/T with the temperature is well described by ansatz (5.4). However, the temperatures we have used are apparently still too low to get in contact with lowest order perturbation theory.

To test the next-to-leading order result (2.26) we also determined the ratio m_e/m_m and especially the magnetic mass. We were only able to extract a reliable result for m_m for the lattice with spatial extension $N_3 = 64$. On the smaller lattice the local screening masses $m_m(x_3, T)$ do not reach a plateau (see App. A.1). Therefore the fits of the correlation function G_m were quite poor, i.e. had a large χ^2. As the electric screening masses obtained from different actions and lattice sizes do not show any significant difference, we expect that also the magnetic mass does not show a significant ultraviolet cut-off dependence.

In Fig. 5.2(a) we show the electric and magnetic screening masses, obtained from the Wilson action simulation on the $32^2 \times 64 \times 8$ lattice. Fig. 5.2(b) gives the squared ratio $(m_e/m_m)^2$. Our data strongly suggest a temperature dependence of the form $(m_e/m_m)^2 \sim g^{\perp 2}(T)$, which is in agreement with the general expectation
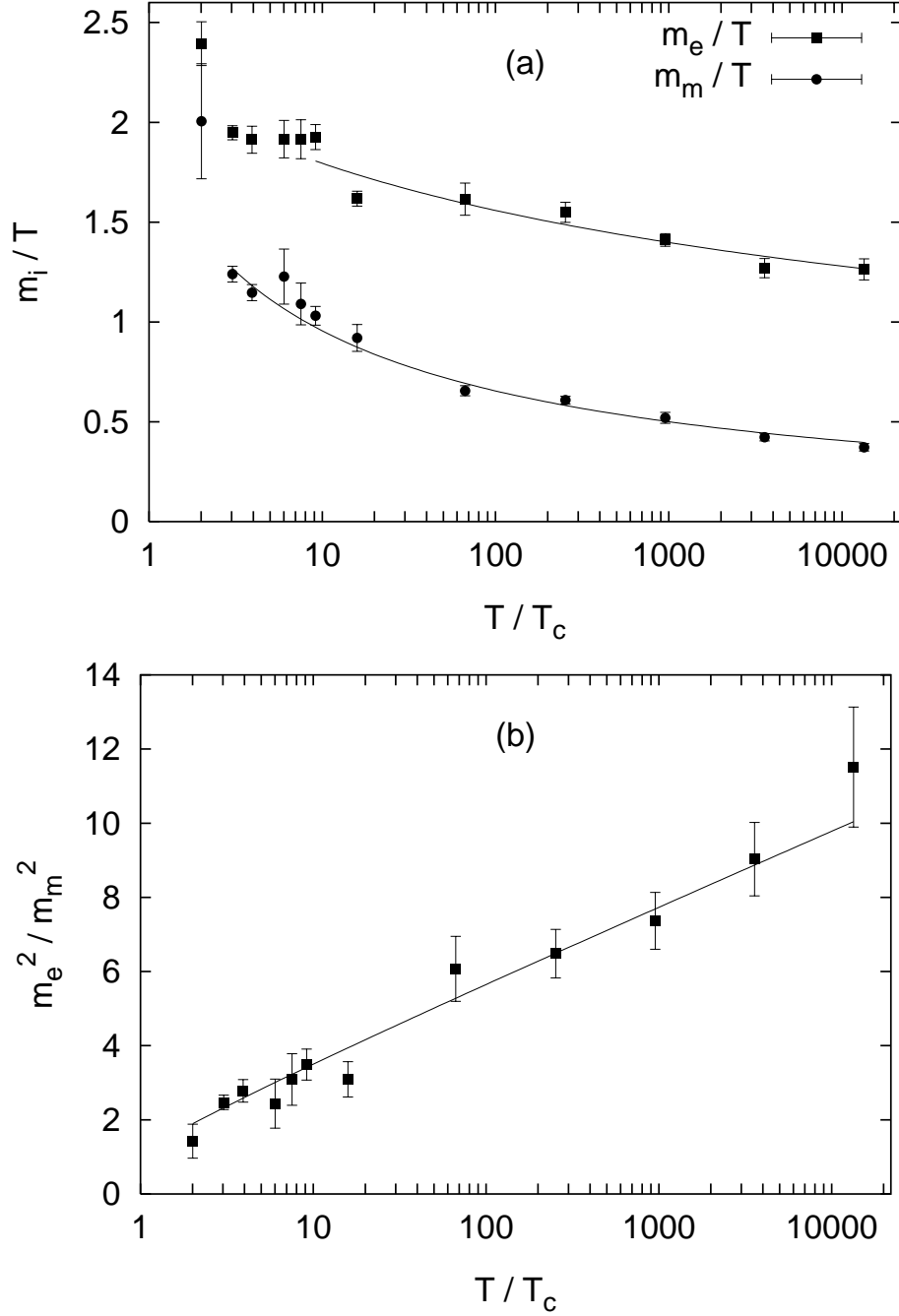
Figure 5.2: Electric and magnetic screening masses in units of the temperature (a) and squared ratio of the masses (b) vs. T/T_c. Data are obtained from simulations on a $32^2 \times 64 \times 8$ lattice using the Wilson action.

$m_m(T) \sim g^2(T)\,T$. We therefore performed a fit according to

$$\left(\frac{m_e(T)}{m_m(T)}\right)^2 = C_{\text{fit}}\; g^{\perp 2}(T) \quad . \tag{5.5}$$

A two parameter fit in the range $T \geq 2\,T_c$ yields $C_{\text{fit}} = 9.16(69)$, $\Lambda_{\text{fit}}/\Lambda_{\overline{\text{MS}}} = 2.42(64)$ with $\chi^2/\text{dof} = 0.79$. Fixing the Λ-parameter to $\Lambda_{\overline{\text{MS}}}$, a one parameter fit results in $C_{\text{fit}} = 7.46(27)$ and $\chi^2/\text{dof} = 1.35$. In Fig. 5.2(b) we have shown the two parameter fit.

With these results at hand we are now able to check the next-to leading order result for m_e. The dashed-dotted line in Fig. 5.1 is a self consistent determination of m_e, using (2.26). It lies about 20% above the lowest order prediction and therefore is closer to our data. However, it is still too low to describe the data well. Therefore we have performed additional fits of the electric mass that take into account higher order corrections. Based on (2.26) we use the ansatz

$$\left(\frac{m_e(T)}{T}\right)^2 = \frac{2}{3}\, g^2(T) \left(1 + \frac{\sqrt{6}}{2\pi}\, g(T) \left[\log\frac{2\,m_e}{m_m} - \frac{1}{2}\right]\right) + B_{\text{fit}}\; g^4(T) \quad . \tag{5.6}$$

As the g^4-correction term leads to a temperature dependence which is too strong within the entire T-interval, we have restricted the fit to very high temperatures, $T \geq 250\,T_c$. A one parameter fit at fixed $T_c/\Lambda_{\overline{\text{MS}}} = 1.06$ gives $B_{\text{fit}} = 0.744(28)$ with $\chi^2/\text{dof} = 4.55$ (dotted line in Fig. 5.1).

Let us now return to the discussion of the magnetic mass. As noted above, the ratio m_e/m_m suggests a magnetic mass of the form $m_m(T) \sim g^2(T)\,T$. Therefore we fitted m_m with the ansatz

$$\frac{m_m(T)}{T} = D_{\text{fit}}\; g^2(T) \quad . \tag{5.7}$$

The two parameter fit of m_m for $T \geq 3\,T_c$ results in $D_{\text{fit}} = 0.478(17)$ and $\Lambda_{\text{fit}}/\Lambda_{\overline{\text{MS}}} = 0.77(14)$ with $\chi^2/\text{dof} = 1.44$. This is in good agreement with our result obtained in [22] for $T < 20\,T_c$. With a fixed Λ-parameter, $T_c/\Lambda_{\overline{\text{MS}}} = 1.06$, we obtain $D_{\text{fit}} = 0.456(6)$ and $\chi^2/\text{dof} = 1.53$. In Fig. 5.2(a) the two parameter fit is shown. The small deviation of the fitted curve from the measured data shows that the magnetic mass indeed is well described by the functional form $m_m(T) \sim g^2(T)\,T$.

We next want to compare our numerical result with the perturbative calculations presented in [66]. A criterion for the system to become magnetically stable yields as a lower bound for the magnetic mass

$$\frac{m_m(T)}{T} \geq \frac{11}{12\,\pi}\, g^2(T) \simeq 0.29\, g^2(T) \quad \text{for } T \to \infty \; . \tag{5.8}$$

Result (5.8) is remarkable for several reasons. First, it coincides with the general expectation for the temperature dependence of the magnetic mass, which is strengthened by our result $m_m(T) = 0.456(6) g^2(T) T$. Second, it has the same order of magnitude as our result. And third, it is smaller than our result, which is necessary for (5.8) to represent a lower bound.

We finally want to point out one more aspect of our analysis of m_m/T and m_e/m_m. It is, of course, consistent with our most straightforward fit to the electric mass, $m_e(T) = \sqrt{1.69(2)} g(T) T$. In contrast to the fit based on ansatz (5.6) this fit describes the data well in the entire temperature range above T_c. This shows that the electric mass has a strong non-perturbative character in the temperature interval we have investigated.

Results for Non-Zero Momenta

Let us briefly discuss the gluon correlation functions at non-zero momenta. As the numerical signal gets lost in statistical noise for large momenta (see (2.3), (2.4) and (5.1)) we only could analyse the cases $k_1 = 1, 2$, i.e. $p_1 a = 2\pi/N_1$, $4\pi/N_1$. Furthermore, we only obtained a reliable result in the electric sector. From Eq. (5.1) we have

$$\sinh^2 \frac{a E_e(p_1)}{2} = \sinh^2 \frac{a m_e}{2} + \alpha \, \sin^2 \frac{a p_1}{2} \quad . \tag{5.9}$$

For m_e we use the result from the calculation at zero momentum. In the limit $T \to \infty$ one expects to find a free particle dispersion relation, i.e. $\alpha \to 1$. In Fig. 5.3 we have plotted α vs. T/T_c . Obviously we do not have sufficient statistics to uncover a temperature dependence of α. Therefore we only quote a value averaged over the temperature interval $T \geq 9 T_c$. We find $\alpha = 0.37(10)$ for $k_1 = 1$ and $\alpha = 0.65(3)$ for $k_1 = 2$. This suggests a quite significant modification of the free particle dispersion relation at low momenta.

5.1.2 The Electric Screening Mass from the Singlet Potential

In Sec. 2.2.2 we presented another method to extract the electric screening mass, based on an investigation of the colour singlet potential. We are interested in this analysis for two reasons:

- A comparison of the electric screening masses from the gauge boson propagator and from the singlet potential provides a consistency check for m_e .
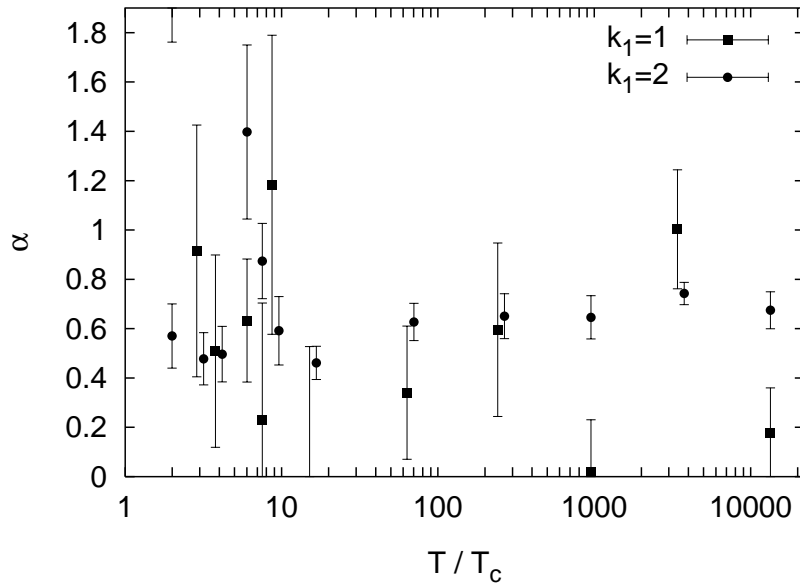
Figure 5.3: α vs. T/T_c for $k_1 = 1, 2$. Some data points have been displaced horizontally for better viewing.

- The singlet potential is a suited candidate at which one can demonstrate the improvement of rotational symmetry due to the use of an improved action.

We will discuss the second point at first.

Improvement of the Singlet Potential

For the investigation of the improvement of the rotational symmetry of the singlet potential we use the point-to-point correlation functions (2.9) and (2.11). We have calculated V_1/T both along an axis, labeled with $(1, 0, 0)$, and along three different off-axis directions, $(1, 1, 0)$, $(1, 1, 1)$, and $(2, 1, 0)$, on a lattice of size $32^3 \times 4$. To make the results from simulations with unimproved and improved action comparable, one has to choose couplings that both correspond to the same temperature. As an example, we use in the following $\beta_W = 3.219$ and $\beta_I = 2.652$. As listed in Tab. 3.1, both couplings correspond to $T \simeq 15.88\,T_c$.

Motivated by Eq. (2.9) and taking into account the periodic boundary conditions, we have performed a correlated fit of the $(1, 0, 0)$ data in the interval $R \in [7, 12]$ (see App. A.1), using the fit function

$$V_{1,\text{fit}}(R, T) = A_{\text{fit}} \left(\frac{e^{\pm m_{\text{fit}} R}}{R} + \frac{e^{\pm m_{\text{fit}} (N_3 \pm R)}}{N_3 - R} \right) \tag{5.10}$$

with $N_3 = 32$. The fit results for both actions are listed in Tab. 5.5. As one can see

fit parameters	$\beta_W = 3.219$	$\beta_I = 2.652$
A_{fit}	-1.49(16)	-1.64(13)
m_{fit}	0.435(16)	0.416(11)
goodness	0.380	0.452
χ^2/dof	1.049	0.918
normalized χ^2 deviation from the $(1,0,0)$ fit		
$(1,1,0)$	2.019	1.457
$(1,1,1)$	1.934	0.090
$(2,1,0)$	1.316	0.243

Table 5.5: Results from the fits of V_1/T at $\beta_W = 3.219$ and $\beta_I = 2.652$ ($T \simeq 15.88\, T_c$).

from the upper part of the table, the fit itself is better for the improved data than for the Wilson data, i.e. the errors on the fit parameters are smaller, the goodness is larger and finally the squared error from the correlated fit (χ^2/dof) is smaller. The lower part of Tab. 5.5 shows the χ^2 deviation of the off-axis data points from the $(1,0,0)$ fit curves. For this comparison we used data in the interval $7 \leq R \leq 12$ and divided by the number of points taken into consideration. For all measured off-axis directions these data show that the violation of rotational symmetry is lowered by going from the Wilson to the tree-level Symanzik improved action. This behaviour becomes also clear from Fig. 5.4, which shows the potential V_1 (normalized by the fit function (5.10) with the parameters given in Tab. 5.5) vs. distance R.

Numerical Results for m_e

We used point-to-point as well as plane-plane Polyakov loop correlation functions to extract the electric screening mass. In the former case we proceeded as mentioned on page 46, i.e. we used Eqs. (2.9) and (2.11) and performed a correlated fit of the numerical data, using (5.10) and the fit criterion described in App. A.1. We did this both for the measurement along the (1,0,0) axis and for the three different off-axis directions previously mentioned. In the second case we obtained m_e from $V_{1,\text{sum}}$, Eqs. (2.12) and (2.13).

Whereas we have calculated $V_{1,\text{sum}}$ on lattices of size $32^3 \times 4$ and $32^2 \times 64 \times 8$ and for both actions, we have calculated V_1 only on the smaller lattice. The results for the electric screening mass are listed in Tab. 5.6 and 5.7.

Similar to the electric mass extracted from gluon correlation functions, the results we have now obtained with different actions and on lattices of varying size again
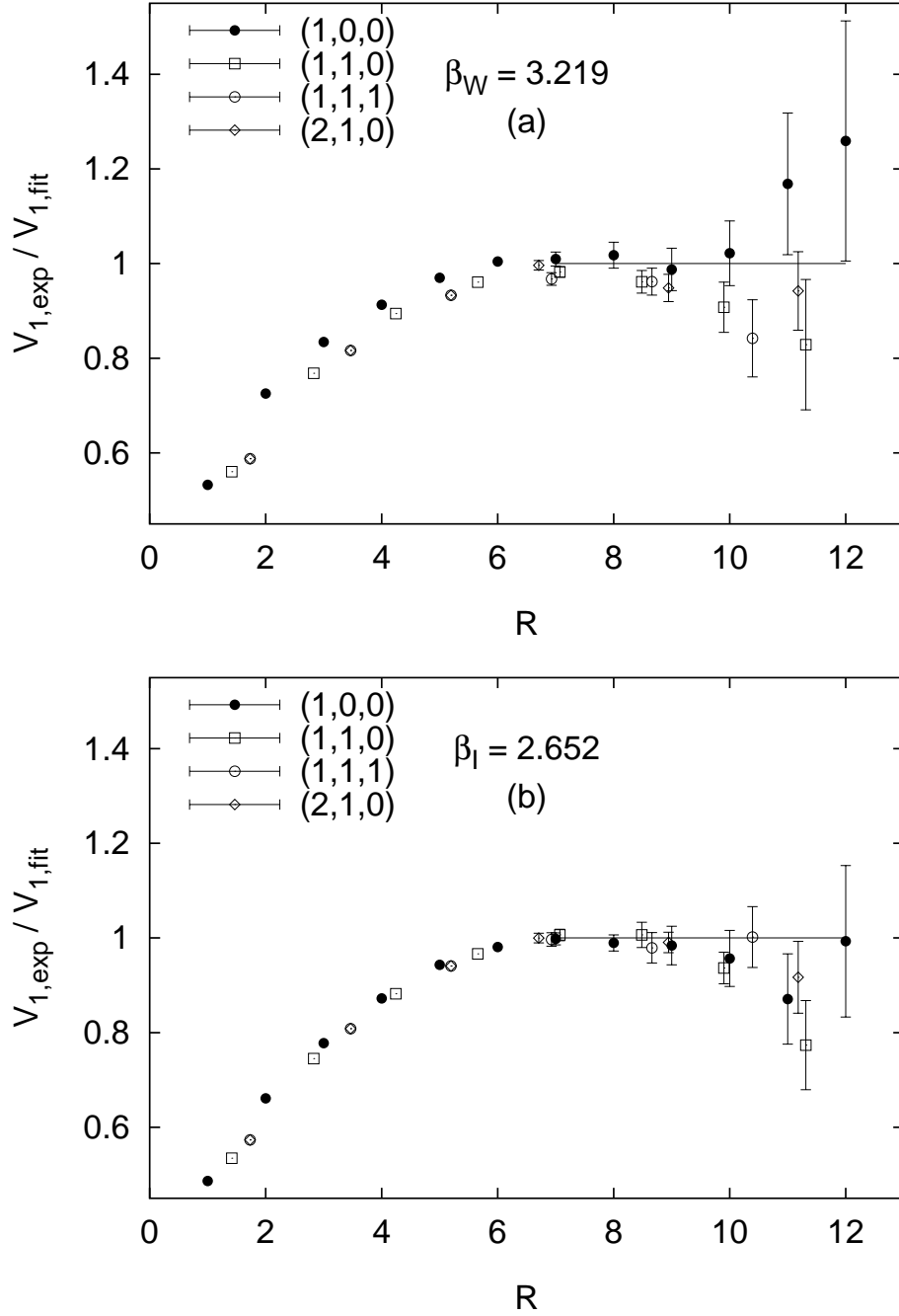
Figure 5.4: Singlet potential $V_1(R)$, normalized by the correlated fit of the $(1,0,0)$-data in the interval $R \in [7,12]$. The data have been calculated on a lattice of size $32^3 \times 4$ using the Wilson action at $\beta_W = 3.219$ (a) and the Symanzik action at $\beta_I = 2.652$ (b). Both couplings correspond to a temperature of $T \simeq 15.88\,T_c$. The different symbols refer to the $(x_1, x_2, x_3)-$directions along which the measurements have been performed.

Wilson action, $32^3 \times 4$ lattice				
β_W	$m_e(T)/T$, extracted from			
	$V_{1,\text{sum}}$	$V_{1,(1,0,0)}$	$V_{1,(1,1,0)}$	$V_{1,(1,1,1)}$	$V_{1,(2,1,0)}$
2.512	2.03(2)	2.28(9)	2.22(4)	2.13(4)	2.38(11)
2.643	2.30(9)	2.15(6)	2.12(5)	2.07(4)	2.25(9)
2.74	2.13(9)	2.09(5)	2.04(5)	2.04(4)	2.14(7)
2.88	2.04(6)	1.95(6)	1.91(3)	1.93(2)	1.96(7)
2.955	1.94(7)	2.11(8)	1.97(5)	1.94(6)	2.06(5)
3.023	2.16(7)	1.84(5)	2.01(4)	1.96(9)	1.98(6)
3.219	1.88(9)	1.74(6)	1.80(4)	1.75(5)	1.83(4)
3.743	1.85(15)	1.50(2)	1.50(1)	1.43(2)	1.61(3)
4.24	1.63(7)	1.55(9)	1.53(7)	1.45(3)	1.44(2)
4.738	1.33(4)	1.75(10)	1.32(5)	1.32(3)	1.29(2)
5.238	1.30(7)	1.29(4)	1.25(4)	1.20(2)	1.19(2)
5.737	1.34(5)	1.29(3)	1.24(4)	1.17(1)	1.15(2)

Symanzik action, $32^3 \times 4$ lattice				
β_I	$m_e(T)/T$, extracted from			
	$V_{1,\text{sum}}$	$V_{1,(1,0,0)}$	$V_{1,(1,1,0)}$	$V_{1,(1,1,1)}$	$V_{1,(2,1,0)}$
1.92	2.26(9)	2.04(4)	2.16(5)	2.12(5)	2.06(2)
2.063	1.97(3)	1.98(3)	2.01(3)	2.03(4)	2.12(7)
2.152	2.07(5)	2.16(8)	2.02(7)	2.04(4)	2.01(6)
2.30	1.93(5)	1.83(2)	1.79(3)	1.70(3)	1.84(4)
2.382	1.82(4)	1.83(3)	1.72(3)	1.70(2)	1.90(5)
2.452	1.78(6)	2.14(12)	1.98(14)	1.76(7)	1.79(5)
2.652	1.69(5)	1.66(4)	1.57(2)	1.54(2)	1.67(3)
3.183	1.65(6)	1.58(6)	1.62(5)	1.51(3)	1.48(2)
3.684	1.38(4)	1.71(12)	1.42(3)	1.36(3)	1.33(2)
4.185	1.62(7)	1.66(15)	1.34(3)	1.19(2)	1.21(66)
4.685	1.46(12)	1.22(3)	1.19(3)	1.10(2)	1.09(1)
5.186	1.16(2)	1.22(5)	1.14(3)	1.05(2)	1.03(1)

Table 5.6: Electric screening masses from Polyakov loop correlation functions.

Wilson action, $32^2 \times 64 \times 8$ lattice					
β_W	$m_e(T)/T$	β_W	$m_e(T)/T$	β_W	$m_e(T)/T$
2.74	2.46(16)	3.20	1.76(4)	4.50	1.55(10)
2.88	1.89(4)	3.27	1.93(5)	5.00	1.36(3)
2.97	1.80(31)	3.47	1.65(3)	5.50	1.18(8)
3.12	1.92(8)	4.00	1.61(4)	6.00	1.16(31)

Table 5.7: Electric screening masses from $V_{1,\text{sum}}$.

do not differ significantly. Therefore we have also here analysed all three datasets together. The screening masses, extracted from $V_{1,\text{sum}}$, are shown in Fig. 5.5.
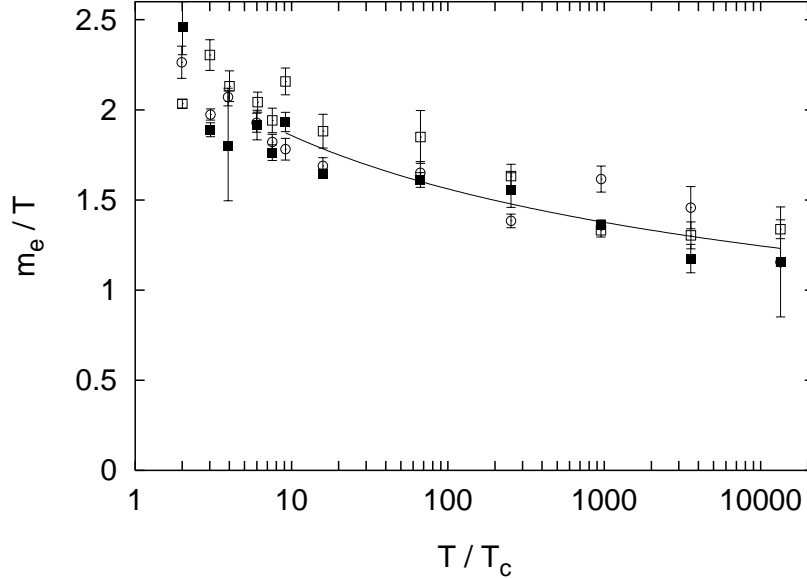
Figure 5.5: Electric screening masses, obtained from $V_{1,\text{sum}}$. The data points refer to the same lattice sizes and actions as in Fig. 5.1. The solid line is a one parameter fit for $T \geq 9\,T_c$, using ansatz (5.4).

As expected from Sec. 5.1, m_e/T, extracted now from Polyakov loop correlation functions, also depends only weakly on the temperature for temperatures less than about $9\,T_c$. For example, fitting $V_{1,\text{sum}}$ in this temperature range with a constant, we obtain $m_e(T)/T = 2.010(13)$.

According to Sec. 5.1 we performed, for temperatures $T \geq 9\,T_c$, one parameter fits (i.e. $\Lambda_{\text{fit}}/\Lambda_{\overline{\text{MS}}} = 1$), using the ansatz (5.4). The results from the lattice of size $32^3 \times 4$

are summarized in Tab. 5.8. On the $32^2 \times 64 \times 8$ lattice we obtain from $V_{1,\text{sum}}$ a fit value $A_{\text{fit}} = 1.72(4)$ with $\chi^2/\text{dof} = 4.60$.

Wilson action, $32^3 \times 4$ lattice					
	Fits of $(m_e(T)/T)^2$, extracted from				
	$V_{1,\text{sum}}$	$V_{1,(1,0,0)}$	$V_{1,(1,1,0)}$	$V_{1,(1,1,1)}$	$V_{1,(2,1,0)}$
A_{fit}	1.97(6)	1.70(3)	1.60(2)	1.53(2)	1.61(2)
χ^2/dof	2.49	10.6	6.64	7.29	4.18

Symanzik action, $32^3 \times 4$ lattice					
	Fits of $(m_e(T)/T)^2$, extracted from				
	$V_{1,\text{sum}}$	$V_{1,(1,0,0)}$	$V_{1,(1,1,0)}$	$V_{1,(1,1,1)}$	$V_{1,(2,1,0)}$
A_{fit}	1.67(4)	1.46(2)	1.46(2)	1.35(2)	1.36(2)
χ^2/dof	7.10	15.0	10.8	4.51	5.72

Table 5.8: Fit results of $(m_e(T)/T)^2$, extracted from Polyakov loop correlation functions, using the fit ansatz (5.4).

In general we find that the results extracted from $V_{1,\text{sum}}$ are in good agreement with the zero momentum results from the gluon correlation functions. To make this clear also quantitatively we have analysed all three datasets for $V_{1,\text{sum}}$ together, as in the case of the gluon correlation functions. The one parameter fit for $T \geq 9T_c$ yields $A_{\text{fit}} = 1.71(2)$ with $\chi^2/\text{dof} = 5.80$. This can be compared with the result from Tab. 5.4, $A_{\text{fit}} = 1.69(2)$ with $\chi^2/\text{dof} = 4.51$. We therefore conclude that the electric screening mass is well described by $m_e(T) = \sqrt{1.70(2)}\, g(T)\, T$ in the temperature range $T \leq 14000\, T_c$.

5.2 The W-Mass in the SU(2)-Gauge-Higgs Model

We have calculated the W-boson screening mass at $\beta_3 = 9.0$ and two different quartic couplings, $\lambda_3 = 0.0485458$ and 0.0523100. At these values of λ_3, which correspond to zero temperature Higgs mases of $m_H \simeq 77$ GeV and 80 GeV, the electroweak phase transition is no longer of first order but has turned into a smooth crossover, see Sec. 4.3. As mentioned in Sec. 2.2.1 we have extracted m_W by measuring the W-boson propagator in Landau gauge. The determination of m_W from the spatial correlation function G_W (see Eq. (2.4)) is done according to the method proposed in App. A.2.

Our calculations have been performed on a $16^2 \times 32$ lattice with very high statistics, see Tab. 5.9. Two measurements, i.e. two consecutive configurations were seperated by 10 update iterations. Each update consists of one heatbath sweep in the gauge field, followed by one heatbath and four overrelaxation sweeps in the Higgs field. Furthermore we use for each Higgs field update a Metropolis accept-reject decision for generating the quartic term in Φ.

We now present our results for m_W. In Figs. 5.6 and 5.7 and Tab. 5.10 we show m_W
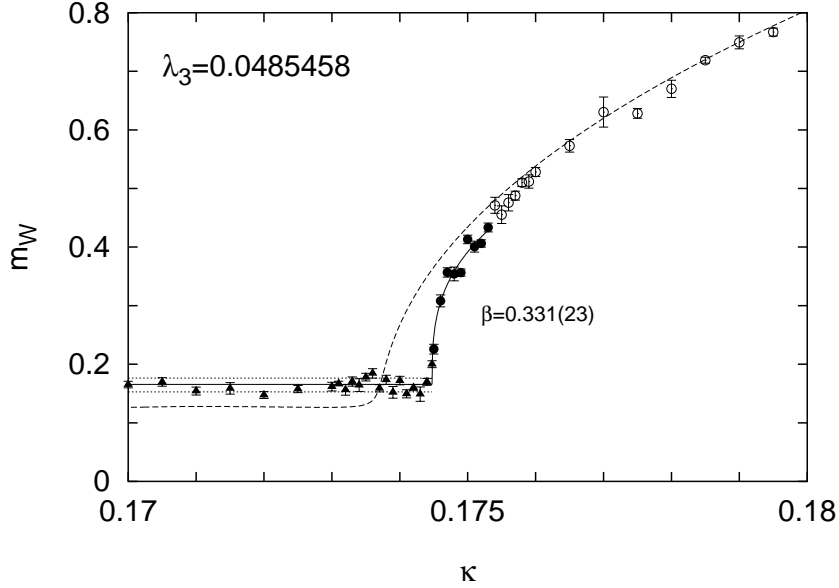
Figure 5.6: W-boson screening mass, calculated on a $16^2 \times 32$ lattice at $\beta_3 = 9.0$ and $\lambda_3 = 0.0485458$. The full curves describe the fits to the data in both phases. The dashed curve represents the result obtained from gap equations. The horizontal dotted lines are the errorband from pure SU(2) gauge theory.

vs. κ at $\lambda_3 = 0.0485458$ and $\lambda_3 = 0.0523100$, respectively. In the symmetric high temperature phase the W-mass stays constant. A fit to the data for $\kappa < \kappa_c{}^1$, the full triangles in both figures, with a constant fitting function yields

$$m_W(\kappa < \kappa_c) = 0.166(2) \quad \text{for} \quad \lambda_3 = 0.0485458 \quad \text{and} \tag{5.11}$$

$$m_W(\kappa < \kappa_c) = 0.162(2) \quad \text{for} \quad \lambda_3 = 0.0523100 \quad . \tag{5.12}$$

Theses values are shown as the horizontal full lines in the figures. They are in excellent agreement with the numerical value of the magnetic screening mass from

---

[1]By calculating the maxima of the Φ^2-susceptibility we determined in [18] the infinite volume critical couplings at $\beta_3 = 9.0$ to be $\kappa_c = 0.1744752(8)$ for $\lambda_3 = 0.0485458$ and $\kappa_c = 0.1746769(9)$ for $\lambda_3 = 0.0523100$, respectively.

$\lambda_3 = 0.0485458$					
κ	# meas.	κ	# meas.	κ	# meas.
0.1700	5000	0.1739	3000	0.1753	5000
0.1705	5000	0.1740	2000	0.1754	6000
0.1710	5000	0.1741	3000	0.1755	4000
0.1715	5000	0.1742	2000	0.1756	4000
0.1720	5000	0.1743	5000	0.1757	2000
0.1725	6000	0.1744	6000	0.1758	2000
0.1730	3000	0.174474	6000	0.1759	2000
0.1731	3000	0.1745	8000	0.1760	4000
0.1732	3000	0.1746	5000	0.1765	4000
0.1733	3000	0.1747	5000	0.1770	2000
0.1734	3000	0.1748	3000	0.1775	4000
0.1735	3000	0.1749	3000	0.1780	2000
0.1736	3000	0.1750	4000	0.1785	4000
0.1737	3000	0.1751	4000	0.1790	2000
0.1738	3000	0.1752	4000	0.1795	4000

$\lambda_3 = 0.0523100$					
κ	# meas.	κ	# meas.	κ	# meas.
0.1700	4000	0.1746	5000	0.1761	5000
0.1705	5000	0.17465	5000	0.1762	5000
0.1710	5000	0.1747	5000	0.1763	5000
0.1715	5000	0.17475	5000	0.1764	5000
0.1720	5000	0.1748	5000	0.1765	5000
0.1725	7000	0.17484	8000	0.1766	5000
0.1730	5000	0.1749	5000	0.1767	5000
0.1735	5000	0.1750	5000	0.1768	5000
0.1736	5000	0.1751	5000	0.1769	5000
0.1737	5000	0.1752	5000	0.1770	5000
0.1738	5000	0.1753	5000	0.1775	1000
0.1739	5000	0.1754	5000	0.1780	1000
0.1740	5000	0.1755	5000	0.1785	1000
0.1741	5000	0.1756	5000	0.1790	1000
0.1742	5000	0.1757	5000	0.1795	1000
0.1743	5000	0.1758	5000	0.1800	1000
0.1744	5000	0.1759	3000		
0.1745	19000	0.1760	5000		

Table 5.9: Number of measurements (SU(2)-gauge-Higgs model on a $16^2 \times 32$ lattice at $\beta_3 = 9.0$).

$\lambda_3 = 0.0485458$					
κ	m_W	κ	m_W	κ	m_W
0.1700	0.165(6)	0.1739	0.152(10)	0.1753	0.433(8)
0.1705	0.170(7)	0.1740	0.172(7)	0.1754	0.471(14)
0.1710	0.154(7)	0.1741	0.150(7)	0.1755	0.455(15)
0.1715	0.159(10)	0.1742	0.160(5)	0.1756	0.476(14)
0.1720	0.147(6)	0.1743	0.149(12)	0.1757	0.488(8)
0.1725	0.158(6)	0.1744	0.170(6)	0.1758	0.510(7)
0.1730	0.162(7)	0.174474	0.200(6)	0.1759	0.512(11)
0.1731	0.167(4)	0.1745	0.226(8)	0.1760	0.528(8)
0.1732	0.156(9)	0.1746	0.308(10)	0.1765	0.573(11)
0.1733	0.170(8)	0.1747	0.357(8)	0.1770	0.630(26)
0.1734	0.164(11)	0.1748	0.354(12)	0.1775	0.628(8)
0.1735	0.178(7)	0.1749	0.356(6)	0.1780	0.670(15)
0.1736	0.184(8)	0.1750	0.413(7)	0.1785	0.719(5)
0.1737	0.159(6)	0.1751	0.401(9)	0.1790	0.749(11)
0.1738	0.173(8)	0.1752	0.406(6)	0.1795	0.767(7)

$\lambda_3 = 0.0523100$					
κ	m_W	κ	m_W	κ	m_W
0.1700	0.167(7)	0.1746	0.169(9)	0.1761	0.508(4)
0.1705	0.159(8)	0.17465	0.184(7)	0.1762	0.500(7)
0.1710	0.157(8)	0.1747	0.212(10)	0.1763	0.526(4)
0.1715	0.155(6)	0.17475	0.260(10)	0.1764	0.523(7)
0.1720	0.164(5)	0.1748	0.295(10)	0.1765	0.529(2)
0.1725	0.151(3)	0.17484	0.308(6)	0.1766	0.554(7)
0.1730	0.171(6)	0.1749	0.318(7)	0.1767	0.541(8)
0.1735	0.157(4)	0.1750	0.348(8)	0.1768	0.567(15)
0.1736	0.166(5)	0.1751	0.366(6)	0.1769	0.570(4)
0.1737	0.164(2)	0.1752	0.404(16)	0.1770	0.569(4)
0.1738	0.141(5)	0.1753	0.389(9)	0.1775	0.603(31)
0.1739	0.151(7)	0.1754	0.405(5)	0.1780	0.654(9)
0.1740	0.160(5)	0.1755	0.446(10)	0.1785	0.676(8)
0.1741	0.174(4)	0.1756	0.429(6)	0.1790	0.706(8)
0.1742	0.145(7)	0.1757	0.442(6)	0.1795	0.713(9)
0.1743	0.167(4)	0.1758	0.479(12)	0.1800	0.767(9)
0.1744	0.173(5)	0.1759	0.453(10)		
0.1745	0.167(6)	0.1760	0.489(13)		

Table 5.10: W-boson screening masses, extracted from a $16^2 \times 32$ lattice at $\beta_3 = 9.0$.
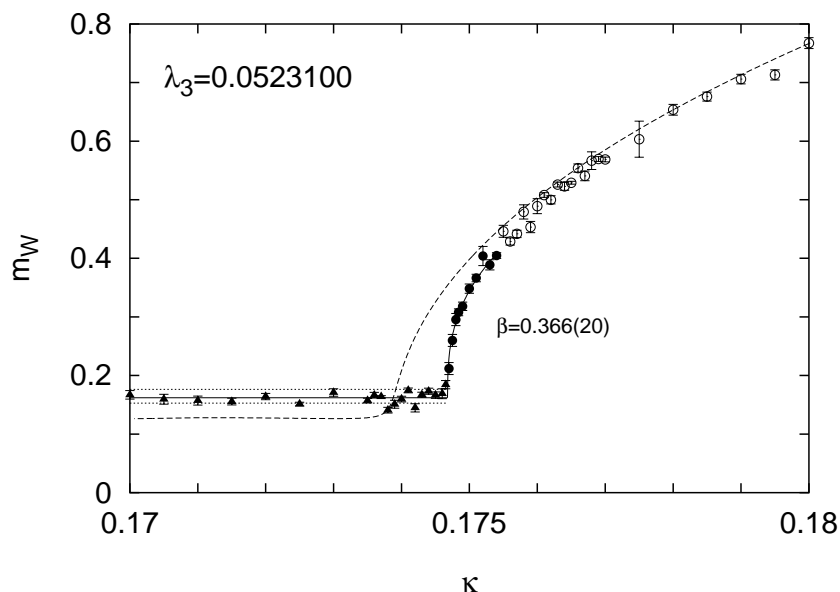
Figure 5.7: Same as Fig. 5.6, now at $\lambda_3 = 0.0523100$.

pure $SU(2)$ gauge theory, $m_m(\beta_3 = 9.0) = 0.165(12)$. Therefore we believe that, in the symmetric phase, the W-boson screening mass is of fully thermal origin, without any high T resp. low κ Higgs effect. The horizontal dotted lines in the figures are the error band corresponding to $m_m(\beta_3 = 9.0)$.

In the symmetry broken low temperature phase ($\kappa > \kappa_c$) the W-boson mass increases rapidly. In this region the data are well described by the ansatz

$$m_W(\kappa > \kappa_c) = m_W(\kappa < \kappa_c) + a\,(\kappa - \kappa_c)^\beta \quad . \tag{5.13}$$

In order to be more sensitive to the critical behaviour near the crossover, we have only fitted data points close to κ_c with ansatz (5.13), the full circles in Figs. 5.6 and 5.7. We obtain

$$a = 2.8(5)\,,\ \ \beta = 0.331(23)\ \ \text{for}\ \ \lambda_3 = 0.0485458 \ \ \text{and} \tag{5.14}$$

$$a = 3.5(6)\,,\ \ \beta = 0.366(20)\ \ \text{for}\ \ \lambda_3 = 0.0523100 \quad . \tag{5.15}$$

The exponent β is close to that of the $O(4)$ spin model in three dimensions. In [67] this exponent has been found to be $\beta = 0.3836(46)$ which is in agreement with results obtained from the $(4 - \epsilon)$-expansion. Through the Higgs-mechanism the W-boson mass in the $SU(2)$-gauge-Higgs model is linked to the scalar field expectation value. It thus seems plausible that also the temperature dependence of the W-boson mass close to κ_c is controlled by the exponent β.

Finally we want to compare our results of the W-mass with the predictions based on gap equations [28, 29, 42], see Sec. 2.3.2. We have solved Eqs. (2.28) - (2.30)

numerically for our set of parameters β_3 (resp. g_3) and λ_3. The results that we have obtained are given by the dashed curves in Figs. 5.6[2] and 5.7. For large values of κ the results from the gap equations agree well with our numerical data.

In the symmetric phase, i.e. below κ_c, the gap equations predict a constant behaviour of m_W. It was found in [28] that for large values of λ_3 the W-boson mass agrees within 10% with the mass obtained from the non-linear σ-model, $m_{\rm SM} = 0.28\, g_3^2$. Furthermore, the W-boson mass was found to be independent in the symmetric phase on λ_3 and κ at large λ_3. This behaviour agrees qualitatively with our results. On a quantitative level, using $g_3 = 2/3$, one has $m_{\rm SM} = 0.124$. This is in rough agreement with the results (5.11) and (5.12).

Near the critical hopping parameter κ_c the results from the gap equations differ from our Monte Carlo data. This behaviour is not unexpected since correlation lengths diverge near κ_c. Therefore both methods only approximate the real W-mass in this region.

So far, we have only discussed the W-boson mass obtained from the W-boson propagator in Landau gauge. In Sec. 2.2.3 we have presented the gauge invariant correlation function G_v (see Eq. (2.17)) that yields the mass of a vector particle with the quantum numbers of the W-boson. This is a suitable candidate that can be compared to the W-mass. However, a detailed analysis of G_v on our data sets failed because the signal disappeared already at rather short distances ($x_3 \simeq 4$) in the statistical noise. The construction of improved operators may help in this channel [41]. To extract some information from the unimproved operator already, we have performed for $\lambda_3 = 0.0523100$ at two κ-values close to κ_c calculations with very high statistics. At $\kappa = 0.1745$ we have made 19000 measurements, at $\kappa = 0.17484$ we have made 8000 measurements, see Tab. 5.9. Fits to the correlation functions G_v for $x_3 \geq 2$ yield

$$m_v \;=\; \begin{cases} 0.557(87) & , \quad \kappa = 0.1745 \\ 0.356(28) & , \quad \kappa = 0.17484 \end{cases} . \tag{5.16}$$

In the symmetric phase at $\kappa = 0.1745$ the mass in the vector channel m_v is more than twice as large as the mass extracted from the W-boson propagator ($m_W = 0.162(2)$). The reason for this might be that the W-boson propagator projects on an one-particle state, whereas the correlation function (2.17) yields the mass from a bounded state of several constituents. In the symmetry broken phase m_W and m_v are similar. For instance, we find from Tab. 5.10 at $\kappa = 0.17484$ for the W-boson propagator mass $m_W = 0.308(6)$, which is compatible with the value given in (5.16) for m_v.

Our calculations of m_W and m_v in the two different phases agree qualitatively with the observations made in [29]. For the symmetry broken phase the authors in [29]

---

[2]We note that Fig. 5.6 is a corrected version of Fig. 4 from [17] in which the gap equations have not been solved correctly.

show that the fluctuations of the Higgs field are small compared to the vacuum expectation value. Therefore the gauge invariant correlation functions are approximately proportional to the corresponding gauge dependent correlation functions [68] and the screening masses, extracted from both types of correlation functions, do roughly agree. For the symmetric phase, however, these arguments do not hold. Therefore the possibility is discussed in [29] that screening masses from gauge invariant correlation functions in this phase correspond to masses of multi-particle states. Especially for the mass in the vector channel a mass formula of the form

$$m_v \simeq 2\,m_\Phi + m_W \tag{5.17}$$

is suggested [29]. Using this relation, our results for m_Φ, as presented in the next section, and m_W would lead to a smaller value of m_v (at $\kappa = 0.1745$). This is not unexpected since (5.17) neglects any binding energies.

5.3 The Higgs-Mass in the SU(2)-Gauge-Higgs Model

In this section we present our numerical data for the Higgs boson screening mass in Landau gauge, obtained from simulations on a $16^2 \times 32$ lattice at $\beta_3 = 9.0$ and $\lambda_3 = 0.0485458$. As explained in Sec. 2.2.4 we have extracted m_Φ from the correlation function $G_\Phi(x_3)$, Eq. (2.20). The results for m_Φ are listed in Tab. 5.11 and shown in Fig. 5.8.

By comparing the Figs. 5.6 and 5.8 one can see that the behaviour of m_Φ is opposite to that of m_W. In the high temperature phase ($\kappa < \kappa_c$) m_Φ drops to zero with increasing κ. This decay is well described by

$$m_\Phi(\kappa < \kappa_c) = a\,(\kappa_c - \kappa)^\nu \quad . \tag{5.18}$$

Fitting the full triangles in Fig. 5.8 with ansatz (5.18) we obtain for the parameters $a = 1.9(2)$ and $\nu = 0.493(30)$.

Slightly above κ_c the screening masses increase. However, our data do not suggest any functional dependence of this behaviour. A further increase of κ seems to leave m_Φ unchanged within statistical errors. A fit of the full circles in Fig. 5.8 results in $m_\Phi(\kappa > 0.1748) = 0.064(2)$.

We present now the results for the screening masses obtained from the scalar correlation functions $\hat{G}_s^{\prime\alpha}(x_3)$ and $\hat{G}_s^{\prime\beta}(x_3)$, Eqs. (2.22) and (2.23). As we have mentioned

κ	m_Φ	κ	m_Φ	κ	m_Φ
0.1700	0.401(11)	0.1739	0.173(17)	0.1753	0.047(17)
0.1705	0.415(21)	0.1740	0.147(11)	0.1754	0.055(10)
0.1710	0.388(11)	0.1741	0.117(10)	0.1755	0.077(7)
0.1715	0.343(13)	0.1742	0.133(9)	0.1756	0.077(6)
0.1720	0.340(13)	0.1743	0.085(11)	0.1757	0.086(11)
0.1725	0.289(10)	0.1744	0.017(3)	0.1758	0.060(13)
0.1730	0.268(8)	0.174474	0.015(1)	0.1759	0.071(14)
0.1731	0.259(11)	0.1745	0.017(9)	0.1760	0.072(11)
0.1732	0.231(16)	0.1746	0.011(8)	0.1765	0.054(8)
0.1733	0.239(10)	0.1747	0.023(11)	0.1770	0.055(14)
0.1734	0.240(9)	0.1748	0.052(7)	0.1775	0.061(11)
0.1735	0.197(10)	0.1749	0.054(9)	0.1780	0.089(9)
0.1736	0.204(30)	0.1750	0.056(8)	0.1785	0.058(14)
0.1737	0.202(14)	0.1751	0.041(11)	0.1790	0.064(13)
0.1738	0.173(12)	0.1752	0.058(11)	0.1795	0.057(13)

Table 5.11: Higgs-boson screening masses, extracted from a $16^2 \times 32$ lattice at $\beta_3 = 9.0$ and $\lambda_3 = 0.0485458$.
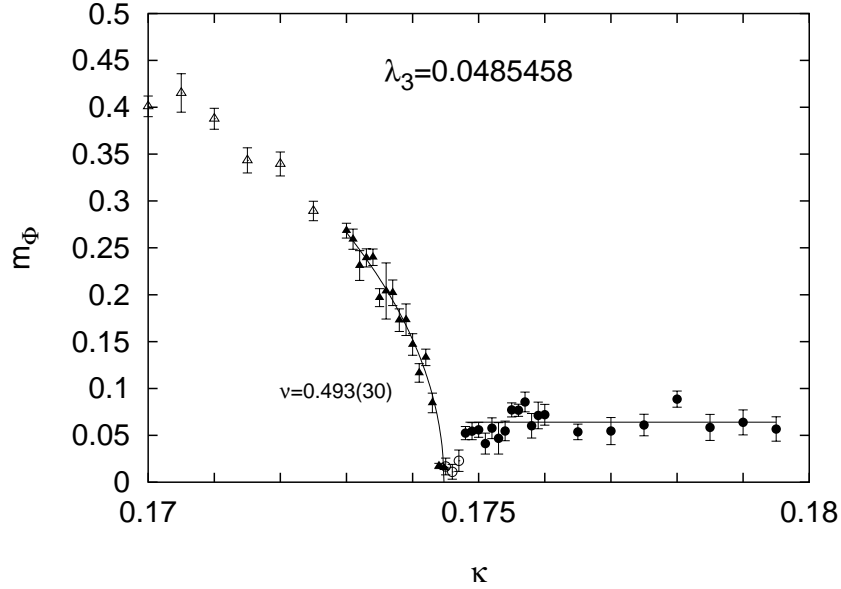

Figure 5.8: The Higgs-mass, calculated on a $16^2 \times 32$ lattice at $\beta_3 = 9.0$ and $\lambda_3 = 0.0485458$. The full curves describe the fits to the data in both phases.

	$\lambda_3 = 0.0485458$		$\lambda_3 = 0.0523100$	
κ	m_s^α	m_s^β	m_s^α	m_s^β
0.1700	1.08(16)	1.24(20)	1.29(10)	1.17(11)
0.1705	1.12(15)	1.12(18)	0.96(15)	0.974(87)
0.1710	0.94(14)	0.944(91)	0.95(14)	0.96(11)
0.1715	0.924(90)	0.878(41)	0.921(70)	0.918(28)
0.1720	0.797(43)	0.849(64)	0.849(84)	0.833(69)
0.1725	0.641(87)	0.617(73)	0.84(10)	0.82(10)
0.1730	0.684(53)	0.635(29)	0.615(67)	0.632(44)
0.1731	0.634(55)	0.620(53)	–	–
0.1732	0.517(41)	0.541(33)	–	–
0.1733	0.594(45)	0.537(45)	–	–
0.1734	0.594(31)	0.608(57)	–	–
0.1735	0.491(37)	0.453(48)	0.724(89)	0.586(38)
0.1736	0.583(31)	0.541(28)	0.475(55)	0.516(45)
0.1737	0.425(32)	0.431(34)	0.545(30)	0.506(39)
0.1738	0.382(40)	0.440(19)	0.479(26)	0.484(25)
0.1739	0.422(29)	0.430(23)	0.477(20)	0.446(28)
0.1740	0.399(66)	0.385(23)	0.432(39)	0.427(36)
0.1741	0.321(25)	0.317(17)	0.430(19)	0.407(17)
0.1742	0.292(25)	0.298(21)	0.319(22)	0.335(14)
0.1743	0.211(12)	0.211(12)	0.322(17)	0.319(14)
0.1744	0.123(11)	0.176(66)	0.274(22)	0.282(21)
0.174474	0.109(9)	0.105(11)	–	–
0.1745	0.129(10)	0.123(9)	0.210(9)	0.211(9)
0.1746	0.169(8)	0.174(7)	0.161(11)	0.153(16)
0.17465	–	–	0.159(22)	0.086(5)
0.1747	0.215(8)	0.210(9)	0.123(29)	0.100(7)
0.17475	–	–	0.171(6)	0.169(5)
0.1748	0.236(18)	0.236(17)	0.183(23)	0.164(14)
0.17484	–	–	0.187(8)	0.187(9)
0.1749	0.275(12)	0.277(12)	0.212(11)	0.211(10)
0.1750	0.262(12)	0.263(13)	0.245(7)	0.244(7)
0.1751	0.294(11)	0.293(11)	0.255(8)	0.253(8)
0.1752	0.307(7)	0.307(7)	0.276(11)	0.274(10)
0.1753	0.309(12)	0.307(13)	0.295(10)	0.295(10)
0.1754	0.327(10)	0.327(10)	0.298(12)	0.297(11)
0.1755	0.339(12)	0.340(10)	0.335(9)	0.333(9)
0.1756	0.359(17)	0.357(17)	0.325(6)	0.326(5)
0.1757	0.381(42)	0.377(19)	0.350(16)	0.348(15)
0.1758	0.370(21)	0.367(13)	0.373(11)	0.373(7)
0.1759	0.360(15)	0.363(16)	0.372(17)	0.369(17)
0.1760	0.408(9)	0.405(10)	0.379(11)	0.380(11)
0.1761	–	–	0.396(13)	0.400(9)
0.1762	–	–	0.386(11)	0.390(16)
0.1763	–	–	0.392(9)	0.391(10)
0.1764	–	–	0.407(18)	0.405(19)
0.1765	0.446(20)	0.446(19)	0.445(16)	0.443(10)
0.1766	–	–	0.429(11)	0.435(7)
0.1767	–	–	0.450(10)	0.449(10)
0.1768	–	–	0.426(19)	0.446(11)
0.1769	–	–	0.465(11)	0.460(9)
0.1770	0.498(37)	0.475(16)	0.466(18)	0.472(11)
0.1775	0.532(14)	0.529(15)	0.582(44)	0.583(38)
0.1780	0.592(25)	0.588(24)	0.659(42)	0.600(19)
0.1785	0.582(29)	0.576(14)	0.565(33)	0.573(31)
0.1790	0.633(14)	0.629(17)	0.646(22)	0.639(23)
0.1795	0.663(17)	0.662(17)	0.616(18)	0.609(15)
0.1800	–	–	0.590(31)	0.587(32)

Table 5.12: Scalar masses, extracted from a $16^2 \times 32$ lattice at $\beta_3 = 9.0$.

in Sec. 2.2.5 these masses are suited to be compared with the Higgs boson screening mass from the Φ-propagator.

Our data for $\lambda_3 = 0.0485458$ and $\lambda_3 = 0.0523100$ are listed in Tab. 5.12. Again, we have used a $16^2 \times 32$ lattice for our simulations. In [16] we have shown that this lattice size is already large enough to avoid finite size effects.

At each λ_3-value, m_s^α and m_s^β are consistent within statistical errors. Therefore we have analysed (at each λ_3-value) both data sets together. In Figs. 5.9 and 5.10 we
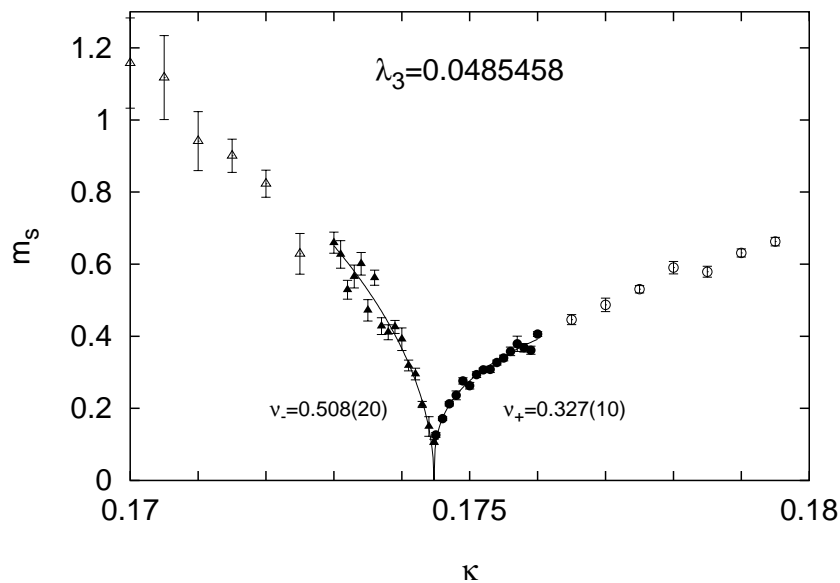

Figure 5.9: Scalar mass, calculated on a $16^2 \times 32$ lattice at $\beta_3 = 9.0$ and $\lambda_3 = 0.0485458$. The full curves describe the fits to the data using ansatz (5.20).

have shown the averaged scalar mass

$$m_s \equiv \frac{1}{2}\left(m_s^\alpha + m_s^\beta\right) \quad . \tag{5.19}$$

A comparison with Fig. 5.8 shows that its behaviour differs strongly from that of m_Φ. Near κ_c the scalar mass becomes very small. This is quite similar to the results obtained from gap equations [28]. However, it was found in [28] that m_s increases faster in the low than in the high temperature phase, in contrast to our results. Furthermore, the critical hopping parameter found in [28] is, as expected from our discussion of the W-boson, smaller than our κ_c. Therefore the dip in Figs. 5.9 and 5.10 is shifted to the left by the analysis of gap equations.

As one can see from the figures, the functional dependence of m_s below and above
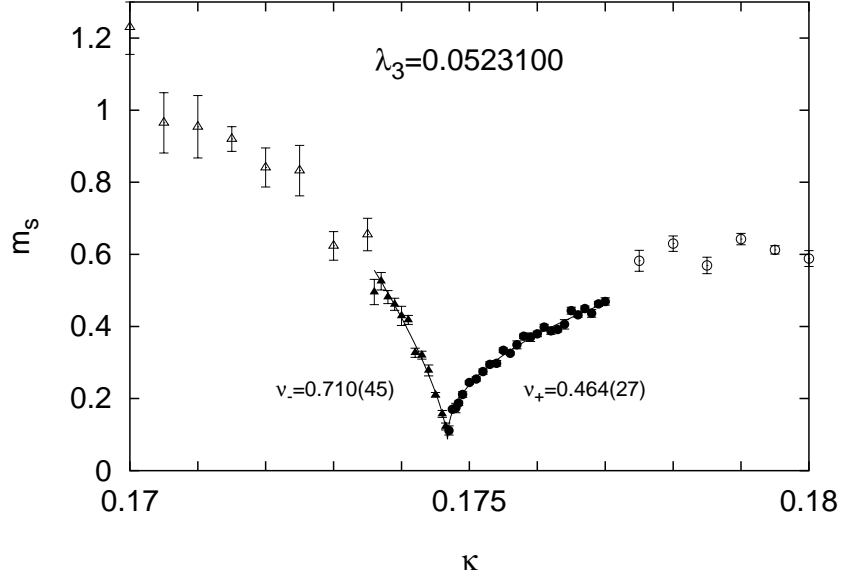
Figure 5.10: Scalar mass, calculated on a $16^2 \times 32$ lattice at $\beta_3 = 9.0$ and $\lambda_3 = 0.0523100$. The full curves describe the fits to the data using ansatz (5.23).

κ_c is clearly different. We therefore have fitted the masses to the ansatz

$$m_s = a_{\pm} |\kappa - \kappa_c|^{\nu_{\pm}} \tag{5.20}$$

where the subscripts +/- refer to the broken/symmetric phases. The results from the two parameter fits of the full triangles resp. circles in the figures are

$$\left. \begin{array}{l} a_{\perp} = 18(2) \;,\; \nu_{\perp} = 0.508(20) \\ a_{+} = 3.3(2) \;,\; \nu_{+} = 0.327(10) \end{array} \right\} \quad \text{for} \quad \lambda_3 = 0.0485458 \quad \text{and} \tag{5.21}$$

$$\left. \begin{array}{l} a_{\perp} = 16(2) \;,\; \nu_{\perp} = 0.500(18) \\ a_{+} = 3.1(1) \;,\; \nu_{+} = 0.315(5) \end{array} \right\} \quad \text{for} \quad \lambda_3 = 0.0523100 \quad . \tag{5.22}$$

The results in [28] open the possibility that m_s is finite at κ_c for the set of parameters chosen by us. Therefore we have performed an additional fit of the scalar masses, allowing in ansatz (5.20) a constant:

$$m_s = c + a_{\pm} |(\kappa - \kappa_c)|^{\nu_{\pm}} \quad . \tag{5.23}$$

Now we find for $\lambda_3 = 0.0485458$

$$\left. \begin{array}{ll} a_{\perp} = 16(2) \;, & \nu_{\perp} = 0.498(13) \\ a_{+} = 3.2(2) \;, & \nu_{+} = 0.321(9) \end{array} \right\} \quad \text{with } c = -0.04(8) \tag{5.24}$$

and for $\lambda_3 = 0.0523100$

$$\left.\begin{array}{ll} a_\perp = 60(19)\ , & \nu_\perp = 0.710(45) \\ a_+ = 6.3(9)\ , & \nu_+ = 0.464(27) \end{array}\right\} \text{ with } c = 0.087(11) \quad . \qquad (5.25)$$

These fit results (5.21) and (5.25) are shown as the solid curves in Figs. 5.9 and 5.10.

For the smaller value of λ_3, i.e. closer to the point where the electroweak phase transition changes from a first order phase transition to a crossover, the additional constant is zero within errors. Therefore we believe that at this λ_3-value the scalar mass is best described by ansatz (5.20). At the larger value of λ_3 we observe a finite constant, in agreement with the predictions made in [28]. To get a more detailed knowledge about the dependence of the constant on λ_3 one would have to perform, of course, much more calculations at several values of λ_3.

Let us make some remarks at this point about the results at $\lambda_3 = 0.0485458$: When approaching κ_c from below (in the symmetric phase) we find that ν is consistent with the mean field value $1/2$. This has also been observed in another simulation of the three dimensional model [40]. However, when approaching κ_c in the broken phase we find a smaller value for the exponent ν. Its numerical value seems to rule out a rather large exponent, i.e. $\nu > 1/2$, like in the 3-d Ising model ($\nu \sim 2/3$) or the $O(4)$-model ($\nu \simeq 0.75$ [67]).

We conclude this section with the comparison of the Higgs boson screening mass, extracted from the Φ-propagator, and the scalar mass at $\lambda_3 = 0.0485458$. In the whole range of κ-values, m_Φ is much smaller than m_s. Similar to the W-boson mass we believe that this is due to the measurement of a single particle mass from the Φ-propagator, whereas we extract masses from composite states by measuring $G_s^{\prime\alpha}$ and G_s^{β}.

On a qualitative level, the behaviour of m_Φ and m_s is similar in the high temperature phase. Both masses are well described by an ansatz $m \sim (\kappa_c - \kappa)^\nu$ with $\nu \simeq 1/2$. The factor of proportionality is, of course, much larger for the scalar mass than for the propagator mass. In the low temperature phase the dependence of m_Φ and m_s on κ differs a lot. While m_Φ seems to be independent of κ, m_s increases with increasing κ.

Chapter 6

Summary and Conclusions

We have studied thermal screening masses in the standard model of strong and electroweak interactions. For the investigation of the strongly coupled sector of the theory we have chosen pure $SU(2)$ gauge theory. Our results for the electroweak sector have been obtained from the dimensional reduced, effective $SU(2)$-gauge-Higgs model.

Let us first summarize the results from pure $SU(2)$ lattice gauge theory. Using the standard Wilson action and a tree-level Symanzik improved action, we have investigated Polyakov loop and gluon correlation functions in a wide range of high temperatures in the deconfined phase. We have calculated chromo-electric and -magnetic screening masses in Landau gauge and have determined their dependence on the temperature.

The temperature dependence found for the magnetic mass is in accordance with the expected $g^2 T$-dependence. We find $m_m(T) = 0.456(6) \, g^2(T) \, T$, which is consistent with the lower bound found in [66], $m_m(T) \geq 11/(12 \, \pi) \, g^2(T) \, T$. For the ratio of the electric and magnetic masses we calculate $(m_e/m_m)^2 = 7.46(27) \, g^{\perp 2}(T)$. Even if this suggests that the temperature dependence of m_e is well described by $m_e \sim gT$ as expected by lowest order perturbation theory, the situation is more complicated. In the temperature range below $10 \, T_c$ we observe a constant behaviour of the electric mass, $m_e/T \simeq 2$. At higher temperatures (up to $10^4 \, T_c$), the temperature dependence of m_e is consistent with a logarithmic dependence, $m_e \sim gT$. However, our data do not agree with lowest order perturbation theory. Only little improvement is achieved by using next-to-leading order results from resummed PT. From an analysis of the gluon propagator as well as the colour singlet potential we find $m_e(T) = \sqrt{1.70(2)} \, g(T) \, T$. This result shows that the screening mechanism is highly non-perturbative even for temperatures as large as $14000 \, T_c$. This observation is in accordance with studies of screening in dimensionally reduced 3d-QCD [23, 24].

Our simulation of the gluon correlation functions at finite momenta still suffer from insufficient statistics. We find a modification of the energy momentum dispersion relation of a free particle, but we are not yet able to quantify its temperature dependence.

The improvement of the action does not show, within statistical errors, any significant modification of the behaviour of the screening masses, although we can show that the violation of the rotational symmetry of the singlet potential, which also was used to extract m_e , is weakened.

In the three dimensional SU(2)-gauge-Higgs model we have calculated the thermal screening masses of the W-boson and of the Higgs boson at couplings $\lambda_3 = 0.0485458$ and 0.0523100, corresponding to zero temperature Higgs masses of $m_H \simeq 77$ GeV and 80 GeV. To extract the screening masses, we have used in both cases the direct measurements of the corresponding propagators in Landau gauge and investigations of gauge invariant correlation functions.

The magnetic screening mass of the W-boson propagator agrees qualitatively with predictions based on gap equations [28]. It remains constant in the symmetric phase and is, within statistical errors, independent on the quartic coupling λ_3. It agrees well with the same quantity of the pure gauge system, $m_m = 0.165(12)$ (at $\beta = 9.0$). This suggests that the high temperature behaviour of the W-boson screening mass is of fully thermal origin and is not influenced by any Higgs type effect.

This equality cannot be a coincidence and gets further support from the study of the gauge invariant excitation spectrum. It is reported in [41] that a 0^{++} state composed of gauge plaquettes does not mix with those operators having the same quantum numbers and also involving Higgs fields. This decoupling phenomenon is actually expected at high temperature. It corresponds to the separation of the heavy scalar modes from the dynamics of the weakly screened magnetic fluctuations which are described by an effective theory both in the case of QCD and the gauge-Higgs system [69].

On the basis of this apparent decoupling we have argued that the magnetic vector fluctuations do not receive any contribution to their screening mass from a Higgs-type mechanism in the high temperature phase. The onset of the additional mass generation through the Higgs-mechanism can be observed as a well-localized increase of the effective mass above κ_c . Our present calculations suggest the existence of a second order phase transition at our sets of couplings. This agrees well with detailed finite size studies of the endpoint of the first order electroweak phase transitions, using Lee-Yang zeros. This method determines the critical quartic coupling to be $\lambda_{3,c} = 0.04795(52)$ (according to a critical Higgs-mass of $m_{H,c} = 75.7(4)$ GeV). The couplings we have used are larger than $\lambda_{3,c}$ and therefore do not correspond to a first order phase transition.

The propagator masses and the gauge invariant spectrum agree well in the symmetry broken phase. An important issue is to clarify why the two kinds of operators, which yield the same mass in the symmetry broken phase, cease to couple to the same state in the symmetric phase. Further investigations of gauge invariant and gauge dependent correlation functions should lead to progress on this question. One possibility would be, for instance, to construct also simple non-gauge invariant two-particle operators whose correlators in Landau gauge could reproduce the results of the gauge invariant spectroscopy.

Opposite to the behaviour of the screening mass of the W-boson propagator is the behaviour of the screening mass of the Higgs boson propagator. In the symmetric phase m_Φ drops to zero with increasing κ. Beyond κ_c it acquires a finite value and remains constant within statistical errors under further heightening of κ. A comparison with the corresponding masses from gauge invariant scalar correlation functions yields, in contrast to the W-boson mass, larger values for the masses in both phases besides κ_c. We believe that one measures here again masses of many particle states. In addition, the functional form of m_s is different from the one of m_Φ. Near κ_c a good description of the scalar screening mass is given by $m_s = c + a_\pm |\kappa - \kappa_c|^{\nu_\pm}$. Close to the endpoint ($\lambda_{3,c} = 0.04795(52)$, i.e. $m_{H,c} = 75.7(4)$ GeV) of the first order electroweak phase transitions we find $c = 0$. For $\nu_\perp = \nu (\kappa < \kappa_c)$ we obtain $\nu_\perp \simeq 1/2$. This agrees with the behaviour of m_Φ slightly below κ_c, $m_\Phi(\kappa < \kappa_c) \sim (\kappa_c - \kappa)^{1/2}$. However, the factor of proportionality is much bigger for m_s than for m_Φ. Above κ_c we find $\nu_+ \simeq 0.32$. At large values of λ_3 ($\lambda_3 = 0.0523100$, i.e. $m_H \simeq 80$ GeV) we calculate $c \simeq 0.09$. For the exponents $\nu_\pm$ we find in this regime $\nu_\perp \simeq 0.71$ and $\nu_+ \simeq 0.46$.

So far, we have only analysed the $SU(2)$-gauge-Higgs model in three dimensions. To check the reliability of dimensional reduction it would be, of course, interesting to perform similar calculations also in four dimensions. Furthermore, studies with improved actions are of interest for getting a taste of the cut-off dependence of the screening masses in the electroweak sector. Work in these directions is in progress.

As mentioned above, we have measured the gauge dependent W-boson and Higgs boson propagators in Landau gauge. The screening masses we have obtained from these correlation functions should be, of course, gauge independent. Therefore it would be interesting to measure the propagators also in a different gauge. A method how to fix the covariant gauge on the lattice was presented in [70]. We discuss the algorithm in App. B.2 and show how to cure the failures made in [70]. Therefore one has now a very powerful tool at hand to realize a whole class of gauges on the lattice which can be used to show the gauge independent character of the screening masses. However, it was until now not possible to fix the covariant gauge efficiently within a numerical simulation. Further work in this direction is still needed.

To conclude, the precise determination of thermal screening masses in this disser-

tation delivers a quantitative description of the dependence of these masses on the temperature. This is a very good basis for further theoretical investigations on the nature of these masses. Especially our data might help in finding a theoretical solution which clarifies quantitatively the problem that masses, extracted from gauge dependent correlation functions, acquire higher values than masses from the corresponding gauge independent correlation functions.

Appendix A

Determination of Screening Masses from Correlation Functions

In the following we will discuss how to obtain screening masses (or energies) from lattice correlation functions. We are interested in the case that the relation between the screening mass and the corresponding correlation function is of the form

$$G_{\text{theor.}}(x_3) = A \cdot \cosh\left\{ m \left(x_3 - \frac{N_3}{2} \right) \right\} \quad \text{for } x_3 \gg 1 \quad . \tag{A.1}$$

One has to find a way how to determine m from a given set of numerical data $G(x_3 = 1), \ldots, G(x_3 = N_3/2)$, using the function $G_{\text{theor.}}$. However, there is no unique rule how to do this.

The most natural way to calculate m is to perform a two parameter fit of (A.1). But one has to take several things into account. First of all we have to handle with the restriction $x_3 \gg 1$. It arises already in the continuum and is needed to project on the ground state with the lowest lying mass. Therefore a fit can not start at $x_3 = 1$. But one has not only to determine the left hand side of the fit interval. Because of numerical noise the signal for $G(x_3)$ gets lost for large values of x_3. As a consequence, also the upper bound of the fit range has to be chosen in an appropriate way. In the next section we describe in detail a criterion that automatically finds the best fit range. We have used it to determine the screening masses from the correlation functions that we measured in the context of the SU(2) gauge theory.

Especially on small lattices the criterion does not always work fine in the sense that the chosen fit range is too small resp. the fit is effected with an insufficient goodness. To avoid this, we present in Sec. A.2 an alternative method for measuring screening masses. It is based on a modification of (A.1) which vanishes with increasing lattice size while leaving the masses unchanged within statistical errors. This method was used to extract the screening masses within the SU(2)-gauge-Higgs model.

A.1   Method I

A fit is in general characterized by several properties, namely χ^2, goodness (Q), degrees of freedom (ϱ) and relative errors of the fit parameters. As χ^2 enters directly into the calculation of Q, it is sufficient to consider only the last three quantities. It is desirable to find a fit with large Q, large ϱ and small relative error on the fit parameter we are interested in, i.e. on m/T. As we want to weigh these three quantities, we are looking for a fit interval with

$$Q^\alpha \cdot \varrho^\beta \cdot \left(\frac{\Delta m}{m}\right)^{\perp \gamma} \to \ \max \quad . \tag{A.2}$$

We have chosen the coefficients to be $\alpha = 9$, $\beta = 1$ and $\gamma = 3$. As we put the largest weight on Q, it sometimes happens that only a very small fit interval is selected by this condition. To avoid this problem, we add the extra condition $\varrho \geq 3$. For a two parameter fit this is equivalent to demand that the fit interval should contain at least 5 points. Finally we require that the fit only considers points $G(x_3)$ with errors less than 50 % of their value. This is to reject points that are dominated by statistical noise.

To see how our fit criterion works we show in Fig. A.1 the electric correlation function
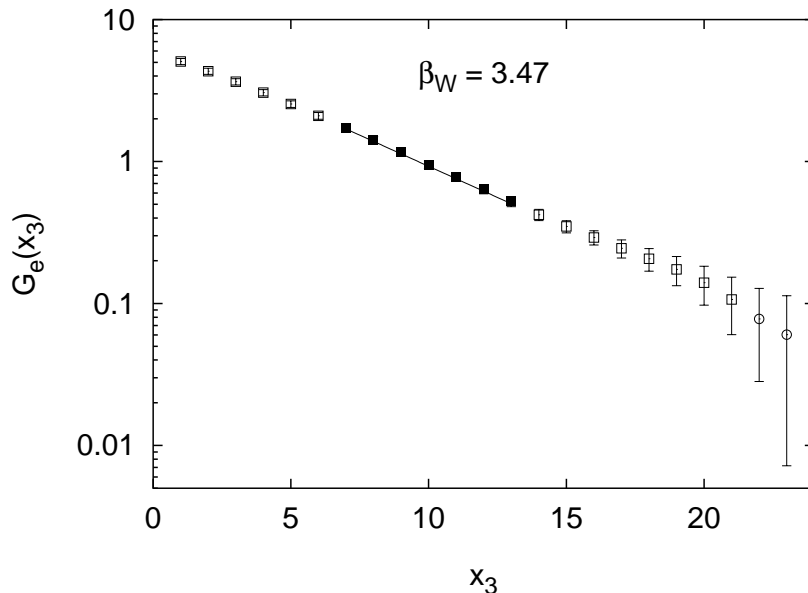

Figure A.1: The electric correlation function $G_e(x_3) \equiv G_e(p_\perp = 0, x_3)$ as a function of x_3. See text for details.

$G_e(p_\perp = 0, x_3)$ (see Eq. (2.3)) as a function of x_3 for the case of pure $SU(2)$ gauge theory, calculated on a lattice of size $32^2 \times 64 \times 8$ for an arbitrary coupling, $\beta_W = 3.47$.

The squares show points with an error less than 50% of the value, whereas the circles describe points with a bigger error. The filled points represent the fit interval, found by our fit criterion. The solid line is the correlated fit found automatically by the fit criterion.

To demonstrate the quality of the fit criterion, we have also studied local screening masses $m(x_3)$. They are defined by the relation

$$\frac{G(x_3)}{G(x_3 + 1)} = \frac{G_{\text{theor.}}(x_3)}{G_{\text{theor.}}(x_3 + 1)} \quad . \tag{A.3}$$

If x_3 becomes large enough, $m(x_3)$ must reach a plateau. On the other hand, if x_3 becomes too large, the local masses have big statistical errors and do not carry valuable information.

In Fig. A.2 we show the local electric screening masses in units of the temperature,
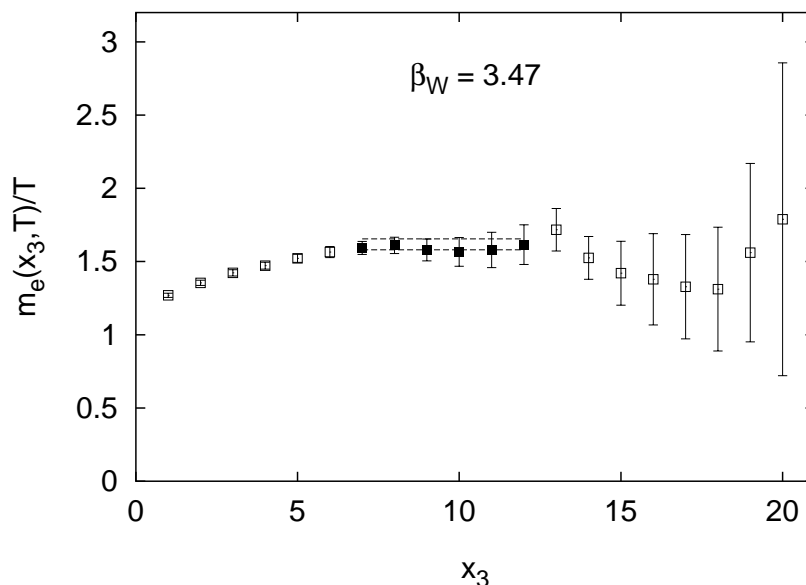

Figure A.2: Local electric screening masses, extracted from the electric correlation function $G_e(x_3)$ shown in Fig. A.1. The horizontal lines are the lower and upper bounds for $m_e(T)/T$, given by the correlated fit shown in Fig. A.1.

$m_e(x_3, T)/T$, extracted from $G_e(x_3)$ shown in Fig. A.1. As a consequence of the slower decay of $G_e(x_3)$ at short distances, which was also observed in [71], the local masses approach a plateau from below at large distance $(x_3 \gtrsim 5)$. The horizontal lines in Fig. A.2 are the lower and upper bounds for $m_e(T)/T$, given by the correlated fit shown in Fig. A.1. Obviously, the fit criterion yields a reliable fit interval.

A.2   Method II

As we have already mentioned, the criterion presented in Sec. A.1 does not always work fine on lattices of small size. Therefore we present now an alternative way how to extract a reliable result for a screening mass from a given correlation function.

The basic idea is to allow in Eq. (A.1) an additional additive parameter,

$$G_{\mathrm{mod.}}(x_3) = A \cdot \cosh\left\{ m \left(x_3 - \frac{N_3}{2} \right) \right\} + B \quad \text{for } x_3 \gg 1 \quad, \tag{A.4}$$

and to perform a three parameter fit of the numerical data. We will in the following show that, for the $SU(2)$-gauge-Higgs model[1], this will minimize the finite size effects in the determination of the screening masses.

To define local screening masses that are independent of B we must modify Eq. (A.3) (which implies $B = 0$):

$$\frac{G(x_3 - 1) - G(x_3)}{G(x_3) - G(x_3 + 1)} = \frac{G_{\mathrm{mod.}}(x_3 - 1) - G_{\mathrm{mod.}}(x_3)}{G_{\mathrm{mod.}}(x_3) - G_{\mathrm{mod.}}(x_3 + 1)} \quad. \tag{A.5}$$

As we are interested in both regions of the electroweak phase transition we have investigated two arbitrary couplings below and above the critical hopping parameter κ_c. At $\lambda_3 = 0.0523100$ and $\beta_3 = 9.0$ (see action (4.7)) we have chosen $\kappa = 0.17450$ (symmetric phase) and $\kappa = 0.17484$ (symmetry broken phase). For these couplings we show in Fig. A.3 the correlation function $G_w(x_3) \equiv G_m(p_\perp = 0, x_3)$ (see Eq. (2.4)) for lattices of size $16^2 \times N_3$, with N_3 ranging from 32 to 128.

For $\kappa = 0.17484$ (Fig. A.3(b)) the datasets of the correlation functions agree well within statistical errors. Therefore we do not measure any finite size effects in the screening masses. This can be seen in the lower part of Tab. A.1 where we show the results of the three parameter fit according to ansatz (A.4). The additional parameter B vanishes within errors, and the result for the screening mass (and also for the factor A) are the same as with ansatz (A.1).

The situation is different in the symmetric phase, Fig. A.3(a). Especially for small N_3 we have large deviations in $G_w(x_3)$. If we analyse the local screening masses according to ansatz (A.3) which implies $B = 0$, the finite size effects in $G_w(x_3)$ result in strong finite size effects in $m_w(x_3)$, see Fig. A.4(a). This situation is improved a lot by using the modified ansatz (A.4). In Fig. A.4(b) we show the local screening masses based on Eq. (A.5). Within errors, the masses extracted from the different

---

[1]Although we have not checked it, the finite size study and its influence on the constant B should also be valid for the pure $SU(2)$ gauge theory.
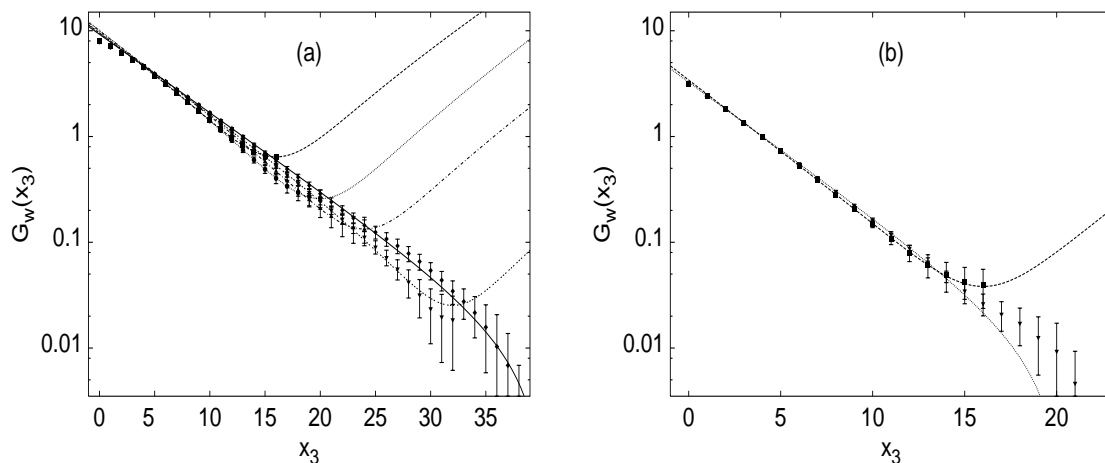
Figure A.3: Gauge field correlation functions on $16^2 \times N_3$ lattices with $N_3 = 32$ (squares), 40 (circles), 48 (upper triangles), 64 (lower triangles) and 128 (diamonds). Shown are correlation functions in the symmetric phase at $\kappa = 0.17450$ (a) and the symmetry broken phase at $\kappa = 0.17484$ (b). The curves give fits for $x_3 \geq 8$. The fitting parameters are listed in Tab. A.1.

lattice sizes are compatible and reach a plateau for distances $x_3 \gtrsim 8$. This behaviour can also be seen in the upper part of Tab. A.1. The finite size effects are absorbed into the parameter B that drops rapidly to zero with increasing lattice size. We find that this decrease is well described by $B \sim \exp\left(-0.1\,N_3\right)$. On the other hand, the fitted values for the screening mass are within errors independent of the volume of the lattice.

We have performed a similar analysis for the dependence of $G_w(x_3)$ on the transverse lattice size. In that case simulations have been performed on lattices of size $N_s^2 \times 32$ with N_s ranging from 4 to 24. Together with the results from this investigation we conclude that the screening masses can reliably be extracted from correlation functions already on lattices of size $16^2 \times 32$ using a fit of the form Eq. (A.4).

$\kappa = 0.17450$				
N_3	m_w	A	B	# iterations
32	0.166(7)	10.3(2)	-0.80(15)	190.000
40	0.194(14)	10.9(6)	-0.18(13)	40.000
48	0.179(11)	10.1(9)	-0.14(8)	40.000
64	0.174(9)	9.3(8)	-0.045(22)	90.000
128	0.163(12)	8.6(9)	-0.012(13)	60.000

$\kappa = 0.17484$				
N_3	m_w	A	B	# iterations
32	0.308(6)	3.4(1)	-0.012(19)	80.000
64	0.291(11)	3.2(2)	-0.009(4)	40.000

Table A.1: Results of fits to the correlation functions shown in Fig. A.3.
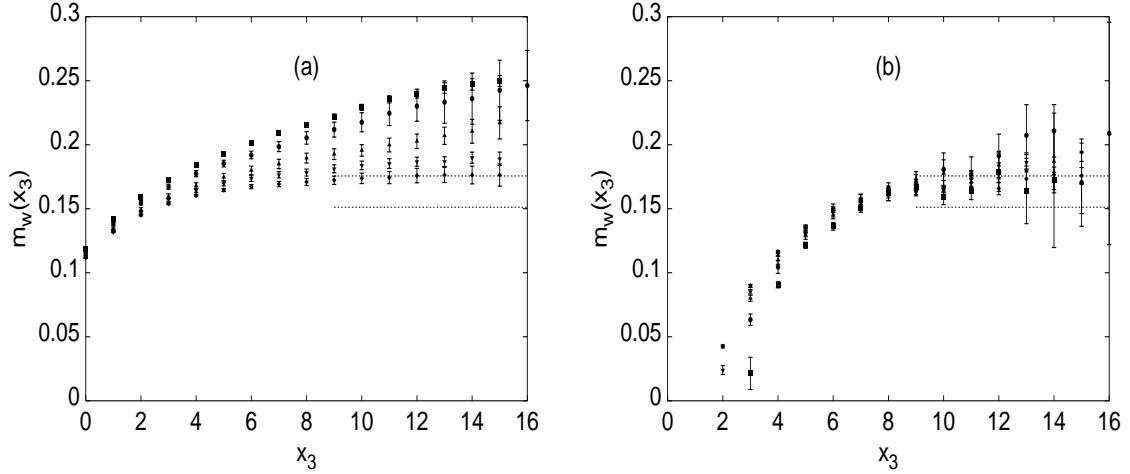

Figure A.4: Local masses calculated at $\kappa = 0.17450$ from the correlation functions shown in Fig. A.3(a). In (a) we show local masses extracted according to Eq. (A.3) while (b) gives the result according to Eq. (A.5). The first one does assume $B = 0$. The horizontal lines give the error band resulting from the fit on a $16^2 \times 128$ lattice.

Appendix B

Lattice Gauge Fixing

A fundamental concept in gauge theories are global and local gauge symmetries. While the action and therefore the "physics" remain invariant under the corresponding gauge transformations, there exist several objects that depend on the gauge, e.g. the fields themselves. Before one can work with these quantities it is therefore necessary to fix a particular gauge.

There exist several gauges in the literature. The gauge we are interested in is the covariant gauge because of its covariant structure. In fact, these gauge corresponds to a whole class of gauges characterized by a continues real parameter $\alpha \geq 0$. This is of great advantage especially if one wants to check the gauge dependence or independence of an observable.

In this work we have only used the Landau gauge $\alpha = 0$ to extract the thermal screening masses. Therefore a future project would be to fix also a general covariant gauge $\alpha \neq 0$ on the lattice, perform the same measurements of the gauge dependent correlation functions and extract again the screening masses. If the concept of screening masses is indeed of real physical than the results obtained in different gauges should be compatible.

So far, however, there are only algorithms known that describe how to fix the Landau gauge on the lattice. They will be summarized in the next section. Very recently there was an article on fixing the covariant gauge on the lattice [70]. We will discuss it in Sec. B.2, point out the failure of the algorithm proposed in [70] and present several ways to cure this defect.

Before we go into the detailed structure of the gauge fixing algorithms we make two general remarks. As the covariant gauge concerns only the gauge fields, its numerical

realization is nearly identical both for pure SU(2) gauge theory and for the SU(2)-gauge-Higgs model. Of course, in the latter one has to gauge update also the Higgs fields at every iteration step, even if this does not effect the gauge condition itself.

Already in the continuum formulation the covariant gauge is not unique. There exist a remaining gauge degree of freedom. This results in so-called Gribov-copies [72]. Furthermore, a lattice gauge fixing algorithm will add more of this artifacts due to numerical uncertainty. Until now it is not completely clarified in how far these ambiguities will effect calculations of gauge dependent objects. In [20] we have investigated the influence of these Gribov-copies on electric and magnetic screening masses in Landau gauge within pure SU(2) gauge theory using the Wilson action. Within statistical errors we did not see any significant shift in the masses for different copies.

B.1   Landau Gauge on the Lattice

In this section we describe how to fix the Landau gauge on the lattice. We follow the approach outlined in [73], [74], [20]-[22].

The task is to find an efficient numerical algorithm to realize the Landau gauge on the lattice. From relation (2.7) we have

$$\partial_\mu A^\mu(x) \simeq \frac{1}{2iag} \sum_{\mu=1}^{N_d} \left(U_\mu(x) - U_\mu^\dagger(x) - U_\mu(x - \hat{\mu}) + U_\mu^\dagger(x - \hat{\mu}) \right) \quad . \qquad (B.1)$$

The gauge condition $|\partial_\mu A^\mu(x)|^2 = 0$ is realized by maximizing the quantity

$$\Sigma \equiv \frac{1}{V} \operatorname{Tr} \sum_x \sum_{\mu=1}^{N_d} \left(U_\mu(x) + U_\mu^\dagger(x) \right) \quad . \qquad (B.2)$$

V is the lattice volume, N_d the number of dimensions.

The most efficient way to bring $\Sigma \to \max$ on each lattice configuration, i.e. the method that consumes the smallest amount of computer time, is to combine two different algorithms. We start with the overrelaxation algorithm [73] up to a numerical accuracy of $|\partial_\mu A^\mu(x)|^2 \leq 10^{\pm 3} - 10^{\pm 5}$, depending on the size of the lattice and the gauge coupling. Due to critical slowing down we then switch to the Fourier accelerated algorithm [74]. We continue gauge fixing until we reach $|\partial_\mu A^\mu(x)|^2 \leq 10^{\pm 9}$. In [20] we have shown that this accuracy is sufficient. Already for $|\partial_\mu A^\mu(x)|^2 \leq 10^{\pm 5}$ the screening masses remain unaffected from further gauge fixing.

Special care has to be taken for the SU(2) gauge theory at temperatures above the critical temperature of the deconfinement phase transition. As already mentioned (see page 28), the system acquires a finite value for the Polyakov loop, $\langle L \rangle \neq 0$. Because of the approximation (2.7) one has to make sure that before starting the gauge fixing algorithm the system is in the phase with $\langle L \rangle > 0$. Because of the global Z(2) symmetry this can be achieved by only one gauge update. Nevertheless, using the wrong phase ($\langle L \rangle < 0$) will result in wrong values for the electric mass!

B.2 Covariant Gauge on the Lattice

A generalization of the Landau gauge is given by the covariant gauge, $|\partial_\mu A^\mu(x) - \Lambda(x)|^2 = 0$. The field $\Lambda(x)$ obeys the probability distribution

$$P(\Lambda(x)) \sim \exp\left\{ -\frac{1}{2\alpha} \mathrm{Tr}\, \Lambda^2(x) \right\} \quad . \tag{B.3}$$

$\alpha = 0$ yields the Landau gauge, $\alpha = 1$ is called Feynman gauge. In the following, we are interested in the case $\alpha \neq 0$.

The realization of the covariant gauge on the lattice will follow at first the ideas outlined in [70]. We will come to the point where the approach in [70] fails and present a modification so that covariant gauge fixing on the lattice should in principle be possible.

Inspired by (B.1), the most straightforward way to fix the covariant gauge on a lattice is to bring the quantity

$$H \equiv \frac{1}{V} \mathrm{Tr} \sum_x \left[\frac{1}{2iag} \sum_{\mu=1}^{N_d} \left(U_\mu(x) - U_\mu^\dagger(x) - U_\mu(x - \hat{\mu}) + U_\mu^\dagger(x - \hat{\mu}) \right) - \Lambda(x) \right]^2 \tag{B.4}$$

towards zero [70].

As $U_\mu(x)$ is an element of the Lie group SU(2) and $\Lambda(x)$ is an element of the Lie algebra su(2), we can use the following parameterizations:

$$U_\mu(x) = a_\mu^4(x)\, \mathbb{1} + i\, \vec{a}_\mu(x)\, \vec{\sigma} \quad \text{with } |a_\mu(x)|^2 = 1 \quad , \tag{B.5}$$

$$\Lambda(x) = \vec{b}(x)\, \vec{\sigma} \quad . \tag{B.6}$$

From Eq. (B.4) we have

$$H = \frac{1}{V} \sum_x \left| \frac{1}{ag} \sum_{\mu=1}^{N_d} \left(\vec{a}_\mu(x) - \vec{a}_\mu(x - \hat{\mu}) \right) \vec{\sigma} - \vec{b}(x)\, \vec{\sigma} \right|^2 \tag{B.7}$$

$$= \frac{1}{Vag} \sum_x \left| \sum_{k=1}^{3} \left\{ \sum_{\mu=1}^{N_d} \left(a_\mu^k(x) - a_\mu^k(x - \hat{\mu}) \right) - ag\, b^k(x) \right\} \sigma^k \right|^2 \qquad (B.8)$$

$$= \frac{1}{Va^2g^2} \sum_x \left| \sum_{k=1}^{3} c^k(x)\, \sigma^k \right|^2 \qquad (B.9)$$

$$= \frac{4}{Va^2g^2} \sum_x \left((c^1(x))^2 + (c^2(x))^2 + (c^3(x))^2 \right) \quad . \qquad (B.10)$$

In (B.9) we defined

$$c^k(x) \equiv \sum_{\mu=1}^{N_d} \left(a_\mu^k(x) - a_\mu^k(x - \hat{\mu}) \right) - ag\, b^k(x) \quad . \qquad (B.11)$$

To obtain $H = 0$ one therefore needs to have

$$c^k(x) = 0 \quad \forall x \text{ and } k = 1, 2, 3 \quad . \qquad (B.12)$$

This is equivalent to

$$b^k(x) = \frac{1}{ag} \sum_{\mu=1}^{N_d} \left(a_\mu^k(x) - a_\mu^k(x - \hat{\mu}) \right) \quad \forall x \text{ and } k = 1, 2, 3 \quad . \qquad (B.13)$$

Using (B.5) we can estimate the right hand side of (B.13). It follows

$$|b^k(x)| \leq \frac{2N_d}{ag} \quad \forall x \text{ and } k = 1, 2, 3 \quad . \qquad (B.14)$$

However, condition (B.14) is in general not satisfied. Using $\sigma^k \sigma^l = \delta^{kl} + i\epsilon^{klm}\sigma^m$, Eq. (B.6) yields

$$\Lambda^2(x) = b^2(x)\mathbb{1} \quad . \qquad (B.15)$$

Inserting this result into (B.3), we obtain for the probability distribution of the lambda matrices

$$P(\Lambda(x)) \sim \exp\left\{ -\frac{1}{\alpha} \left((b^1(x))^2 + (b^2(x))^2 + (b^3(x))^2 \right) \right\} \qquad (B.16)$$

$$= \prod_{k=1}^{3} \exp\left\{ -\frac{1}{\alpha}(b^k(x))^2 \right\} \quad . \qquad (B.17)$$

This means that every $b^k(x)$ is Gauss distributed. Therefore one can not assume that for each lattice side x and for each $k = 1, 2, 3$ the gauge condition (B.14) holds, which means that one can not fix the covariant gauge on a lattice without modification.

Our first proposal to modify the covariant gauge is to create the b^k's according to a "cutted" Gauss distribution. This means that the b^k's will be distributed with

the Gaussian weight (B.17) and underlie the additional restriction (B.14) or an even stronger restriction.

A second possibility is to redefine the Λ-matrix on the lattice [75]. Inspired by relation (2.6) we define

$$U_\Lambda(x) \equiv \frac{1}{iga} \left(1\!\!1 - \exp\{-iga\Lambda(x)\} \right) \quad .$$ (B.18)

Using $U_\Lambda(x)$ instead of $\Lambda(x)$ in (B.4) it should (in principle) be possible to realize the covariant gauge fixing procedure on the lattice.

It remains to quote that in the continuum limit, i.e. for $a \to 0$, both modified gauge proposals result again in the covariant gauge.

Bibliography

[1] S.L. Glashow, Nucl. Phys. **B22** (1961) 579.

[2] S. Weinberg, Phys. Rev. Lett. **19** (1967) 1264.

[3] A. Salam, Proc. 8th Nobel Symposium, edited by N. Svartholm (Almquist und Wiskell, Stockholm 1968).

[4] I. Montvay and G. Münster, *Quantum Fields on a Lattice*, Cambridge University Press (1994).

[5] K.G. Wilson, Phys. Rev. **D10** (1974) 2445.

[6] M. Creutz, Phys. Rev. **D21** (1980) 2308.

[7] K. Rummukainen, Nucl. Phys. B (Proc. Suppl.) 53 (1997) 30.

[8] A.D. Linde, Phys. Lett. **B96** (1980) 289.

[9] A.K. Rebhan, Phys. Rev. **D48** (1993) R3967.

[10] A.K. Rebhan, Nucl. Phys. **B430** (1994) 319.

[11] J.R. Espinosa, M. Quirós and F. Zwirner, Phys. Lett. **B314** (1993) 206.

[12] W. Buchmüller, Z. Fodor, T. Helbig and D. Walliser, Ann. Phys. (N.Y.) **234** (1994) 260.

[13] U.M. Heller, F. Karsch and J. Rank, *Screening Lengths in SU(2) Gauge Theory at Finite Temperature*, contribution to the proceedings of the conference "Strong and Electroweak Matter '97", 21-25 May 1997, Eger, Hungary, hep-lat/9708009.

[14] U.M. Heller, F. Karsch and J. Rank, *Screening Masses and Improvement in Pure SU(2) Lattice Gauge Theory at High Temperatures*, contribution to the proceedings of the conference "Lattice 97, XVth International Symposium on Lattice Field Theory", 22-26 July 1997, Edinburgh, Scotland, hep-lat/9709065.

[15] U.M. Heller, F. Karsch and J. Rank, *The Gluon Propagator at High Temperature: Screening, Improvement and Non-Zero Momenta*, accepted for publication in Phys. Rev. **D**, hep-lat/9710033.

[16] F. Karsch, T. Neuhaus, A. Patkós and J. Rank, Nucl. Phys. **B474** (1996) 217.

[17] F. Karsch, T. Neuhaus, A. Patkós and J. Rank, Nucl. Phys. B (Proc. Suppl.) 53 (1997) 623.

[18] F. Karsch, T. Neuhaus, A. Patkós and J. Rank, in preparation; F. Karsch, T. Neuhaus, A. Patkós, J. Rank and A. Seyfried, in preparation.

[19] See for example J.I. Kapusta, *Finite Temperature Field Theory*, Cambridge University Press 1989.

[20] J. Rank, diploma thesis, University of Bielefeld, 1995.

[21] F. Karsch and J. Rank, Nucl. Phys. B (Proc. Suppl.) 42 (1995) 508.

[22] U.M. Heller, F. Karsch and J. Rank, Phys. Lett. **B355** (1995) 511.

[23] K. Kajantie, M. Laine, K. Rummukainen and M. Shaposhnikov, Nucl. Phys. **B503** (1997) 357.

[24] K. Kajantie, M. Laine, J. Peisa, A. Rajantie, K. Rummukainen and M. Shaposhnikov, *High-T QCD and Dimensional Reduction: Measuring the Debye Mass*, contribution to the proceedings of the conference "Lattice 97, XVth International Symposium on Lattice Field Theory", 22-26 July 1997, Edinburgh, Scotland, hep-lat/9709024.

[25] D.J. Gross, R.D. Pisarski and L.G. Yaffe, Rev. Mod. Phys. **53** (1981) 43.

[26] J.-P. Blaizot and E. Iancu, Nucl. Phys. **B459** (1996) 559.

[27] O. Philipsen, *On the Problem of the Magnetic Mass*, in the proceedings of the NATO Advanced Research Workshop on Electroweak Physics and the Early Universe, March 1994, Sintra, Portugal.

[28] W. Buchmüller and O. Philipsen, Nucl. Phys. **B443** (1995) 47.

[29] W. Buchmüller and O. Philipsen, Phys. Lett. **B397** (1997) 112.

[30] K. Kajantie and J. Kapusta, Phys. Lett. **B110** (1982) 299.

[31] O.K. Kalashnikov, Phys. Lett. **B279** (1992) 367.

[32] F. Karsch, A. Patkós and P. Petreczky, Phys. Lett. **B401** (1997) 69.

[33] G. Boyd, J. Engels, F. Karsch, E. Laermann, C. Legeland, M. Lütgemeier and B. Petersson, Nucl. Phys. **B469** (1996) 419.

[34] R. Kobes, G. Kunstatter and A. Rebhan, Phys. Rev. Lett. **64** (1990) 2992.

[35] R. Kobes, G. Kunstatter and A. Rebhan, Nucl. Phys. **B355** (1991) 1.

[36] P. Arnold and L. G. Yaffe, Phys. Rev. **D52** (1995) 7208.

[37] B. Grossmann, S. Gupta, U.M. Heller and F. Karsch, Nucl. Phys. **B417** (1994) 289.

[38] Z. Fodor, J. Hein, K. Jansen, A. Jaster and I. Montvay, Nucl. Phys. **B439** (1995) 147.

[39] M. Ilgenfritz, J. Kripfganz, H. Perlt and A. Schiller, Phys. Lett. **B356** (1995) 561.

[40] K. Kajantie, M. Laine, K. Rummukainen and M. Shaposhnikov, Nucl. Phys. **B466** (1996) 189.

[41] O. Philipsen, M. Teper and H. Wittig, Nucl. Phys. **B469** (1996) 445.

[42] O. Philipsen, in *Electroweak Physics and the Early Universe*, edited by J.C. Romao and F. Freire, NATO ASI Series B: Physics Vol. 338, (Plenum Press, 1994) 393.

[43] L.D. McLerran and B. Svetitsky, Phys. Rev. **D24** (1981) 450.

[44] I. Montvay, Phys. Lett. **B150** (1985) 441.

[45] I. Montvay, Nucl. Phys. **B269** (1986) 170.

[46] H.Th. Elze, K. Kajantie and J. Kapusta, Nucl. Phys. **B304** (1988) 832.

[47] J. Engels, F. Karsch and H. Satz, Nucl. Phys. **B205** (1982) 239.

[48] B. Beinlich, F. Karsch and E. Laermann, Nucl. Phys. **B462** (1996) 415.

[49] M. Laine, Nucl. Phys. **B451** (1995) 484.

[50] J. Engels, F. Karsch and K. Redlich, Nucl. Phys. **B435** (1995) 295.

[51] J. Fingberg, U.M. Heller and F. Karsch, Nucl. Phys. **B392** (1993) 493.

[52] G. Cella, G. Curci, R. Tripiccione and A. Vicere, Phys. Rev. **D49** (1994) 511.

[53] W. Bernreuther and W. Wetzel, Phys. Lett. **B132** (1983) 382; P. Weisz and R. Wohlert, Nucl. Phys. **B236** (1984) 397; **B247** (1984) 544(E).

[54] R. Dashen and D.J. Gross, Phys. Rev. **D23** (1981) 2340.

[55] F. Karsch, *Simulating the Quark-Gluon Plasma on the Lattice*, in *Quark-Gluon Plasma*, edited by R.C. Hwa, Advanced Series on Directions in High Energy Physics, Vol. 6 (World Scientific, Singapore, 1990) 61.

[56] B. Svetitsky and L.G. Yaffe, Nucl. Phys. **B210** (1982) 423.

[57] J. Engels, J. Fingberg and M. Weber, Nucl. Phys. **B332** (1990) 737.

[58] B. Svetitsky and L.G. Yaffe, Phys. Rev. **D26** (1982) 963.

[59] M. Fukugita, M. Okawa and A. Ukawa, Nucl. Phys. **B337** (1990) 181.

[60] J. Engels, S. Mashkevich, T. Scheideler and G. Zinovjev, Phys. Lett. B365 (1996) 219.

[61] A.M. Ferrenberg and D.P. Landau, Phys. Rev. **B44** (1991) 5081.

[62] K. Farakos, K. Kajantie, K. Rummukainen and M. Shaposhnikov, Nucl. Phys. **B425** (1994) 67.

[63] K. Farakos, K. Kajantie, K. Rummukainen and M. Shaposhnikov, Nucl. Phys. **B442** (1995) 317.

[64] A. Jakovác and A. Patkós, Nucl. Phys. **B494** (1997) 54.

[65] C.N. Yang and T.D. Lee, Phys. Rev. **87** (1952) 404.

[66] V.L. Eletsky, A.C. Kalloniatis, F. Lenz and M. Thies, *Magnetic and Thermo-dynamic Stability of SU(2) Yang-Mills Theory*, hep-ph/9711230 v2.

[67] K. Kanaya and S. Kaya, Phys. Rev. **D51** (1995) 2404.

[68] J. Fröhlich, G. Morchio and F. Strocchi, Nucl. Phys. **B190** [FS3] (1981) 553.

[69] E. Braaten, Phys. Rev. Lett. **74** (1995) 2164.

[70] L. Giusti, Nucl. Phys. **B498** (1997) 331.

[71] A. Nakamura, H. Aiso, M. Fukuda, T. Iwamiya, T. Nakamura and M. Yoshida, *Gluon Propagators and Confinement*, in *Confinement 95*, edited by H. Toki et al., (World Scientific, 1995) 90.

[72] V.N. Gribov, Nucl. Phys. **B139** (1978) 1.

[73] J.E. Mandula and M. Ogilvie, Phys. Lett. **B201** (1988) 117 and Phys. Lett. **B248** (1990) 156.

[74] C.T.H. Davies, G.G. Batrouni, G.R. Katz, A.S. Kronfeld, G.P. Lepage, K.G. Wilson, P. Rossi and B. Svetitsky, Phys. Rev. **D37** (1988) 1581.

[75] B. Berg, private communication.

Curriculum Vitae

Personal Data:

Surname:	Rank
First Name:	Jörn Karl Thies
Address:	Fakultät für Physik, Universität Bielefeld, P.O. Box 100131, 33501 Bielefeld, Germany
Date of Birth:	13.03.1969
Place of Birth:	Bielefeld
Marital Status:	Married with Christiane Rank, née Coors
Citizenship:	Federal Republic of Germany

Educational Background:

May 1988	High school Examination (Abitur), Grade *1.5*
Oct. 1989	Enrollment at the Dept. of Physics of the University of Bielefeld
March 1995	Physics Diploma, Grade *ausgezeichnet*
	Diploma Thesis under the Supervision of Prof. Dr. F. Karsch.
	Title (in German): *Eichabängige Korrelationsfunktionen in der Hochtemperaturphase der reinen SU(2)-Gittereichtheorie*
April 1995 - Jan. 1998	Graduate Student at the University of Bielefeld under the Supervision of Prof. Dr. F. Karsch
June 1996 - May 1997	Visit at the Supercomputer Computations Research Institute (SCRI) at the Florida State University, Tallahassee, Florida, USA. Collaboration with Dr. U.M. Heller as part of the PhD-Studies

Fellowships, Scholarships:

28.07. - 26.08.1994	TRACS-Scholarship at EPCC, University of Edinburgh, Scotland
15.09. - 10.11.1995	TRACS-Scholarship at EPCC, University of Edinburgh, Scotland
Oct. '95 - Sept. 1997	Fellowship of the Land North Rhine-Westfalia
June '96 - May 1997	Fellowship of the German Academic Exchange Service (DAAD) to study in Tallahassee, USA

International Conferences and Workshops:

14.06. - 16.06.1993	"Large Scale Computational Physics on Massively Parallel Computers", Höchstleistungsrechenzentrum (HLRZ), Jülich, Germany
27.09. - 01.10.1994	Poster at "Lattice 94, XIIth International Symposium on Lattice Field Theory", Bielefeld

17.05.-18.05.1996	"The Quark, the Plasma and Beyond", Center for Interdisciplinary Research (ZiF), Bielefeld
03.06.-09.06.1996	Talk at "Lattice 96, XIVth International Symposium on Lattice Field Theory", St. Louis, USA
22.07.-26.07.1997	Talk at "Lattice 97, XVth International Symposium on Lattice Field Theory", Edinburgh, Scotland
30.07.-01.08.1997	Talk at the 2nd German-Japanese Workshop on "The Simulation of Quantum Field Theory on Massively Parallel Computers", Center for Interdisciplinary Research (ZiF), Bielefeld

List of Publications:

Publications:

(1) *The Gluon Propagator at High Temperature* (with U.M. Heller and F. Karsch), Phys. Lett. **B355** (1995) 511.

(2) *Gauge Boson Masses in the 3-d, SU(2) Gauge-Higgs Model* (with F. Karsch, T. Neuhaus and A. Patkós), Nucl. Phys. **B474** (1996) 217.

(3) *The $\mathcal{O}(g^6)$ Coefficient in the Thermodynamic Potential of Hot SU(N) Gauge Theories and MQCD* (with F. Karsch, M. Lütgemeier and A. Patkós), Phys. Lett. **B390** (1997) 275.

(4) *The Gluon Propagator at High Temperature: Screening, Improvement and Non-Zero Momenta* (with U.M. Heller and F. Karsch), accepted for publication in Phys. Rev. D, hep-lat/9710033.

Contributions to Conferences:

(1) *Landau Gauge Fixing and Finite Temperature Gluon Propagator in SU(2) Lattice Gauge Theory* (with F. Karsch), Nucl. Phys. B (Proc. Suppl.) 42 (1995) 508.

(2) *Critical Higgs Mass and Temperature Dependence of Gauge Boson Masses in the SU(2) Gauge-Higgs Model* (with F. Karsch, T. Neuhaus and A. Patkós), Nucl. Phys. B (Proc. Suppl.) 53 (1997) 623.

(3) *The Non-Perturbative $\mathcal{O}(g^6)$ Contribution to the Free Energy of Hot SU(N) Gauge Theory* (with F. Karsch, M. Lütgemeier and A. Patkós), Nucl. Phys. B (Proc. Suppl.) 53 (1997) 417.

(4) *Screening Lengths in SU(2) Gauge Theory at Finite Temperature* (with U.M. Heller and F. Karsch), contribution to the proceedings of the conference "Strong and Electroweak Matter '97", 21.05.-25.05.1997, Eger, Hungary, hep-lat/9708009.

(5) *Screening Masses and Improvement in Pure SU(2) Lattice Gauge Theory at High Temperatures* (with U.M. Heller and F. Karsch), contribution to the proceedings of the conference "Lattice 97, XVth International Symposium on Lattice Field Theory", 22.07.-26.07.1997, Edinburgh, Scotland, hep-lat/9709065.

Acknowledgments:

This dissertation was performed at the University of Bielefeld under the excellent supervision of Prof. Dr. F. Karsch. I would like to thank Prof. Karsch very much for several hours of fruitful discussion and his patience in answering lots of even boring questions.

A lot of work concerning the electroweak simulations was done in collaboration with Dr. T. Neuhaus. I thank him deeply for hours of very interesting discussions, especially during our common time in Tallahassee.

Furthermore I thank Dr. U.M. Heller for his kind hospitality during my one year visit at the Supercomputer Computations Research Institute in Tallahassee.

Financial support of a fellowship from North Rhine-Westphalia (Stipendium nach dem Graduiertenförderungsgesetz des Landes Nordrhein-Westfalen) is gratefully acknowledged.

I thank the staff from the HLRZ in Jülich, the University of Wuppertal, the EPCC in Edinburgh and the SCRI in Tallahassee for their kind permission to use their supercomputers.

My special thank is dedicated to my parents for their support during all the years of my studies and, last but not least, to my wife Christiane for her love and for her patience during the time of writing this thesis. In addition, I owe the finding of several spelling mistakes to her.

Bielefeld, January 16, 1998

(Jörn Rank)